

Managing Singular Kernels and Logarithmic Corrections in the Staggered Six-Vertex Model

Mouhcine Azhari^{1,2} and Andreas Klümper¹

¹Department of Physics, University of Wuppertal, Gausstraße 20, 42119 Wuppertal, Germany

²École Royale Navale, Casablanca 20052, Morocco

azhari.mouhcine@gmail.com, kluemper@uni-wuppertal.de

December 10, 2024

Abstract

In this paper, we investigate the spectral properties of the staggered six-vertex model with \mathbb{Z}_2 symmetry for arbitrary system sizes L using non-linear integral equations (NLIEs). Our study is motivated by two key questions: what is the accuracy of results based on the ODE/IQFT correspondence in the asymptotic regime of large system sizes, and what is the optimal approach based on NLIE for analyzing the staggered six-vertex model?

We demonstrate that the quantization conditions for low-lying primary and descendant states, derived from the ODE/IQFT approach in the scaling limit, are impressively accurate even for relatively small system sizes. Specifically, in the anisotropy parameter range $\pi/4 < \gamma < \pi/2$, the difference between NLIE and ODE/IQFT results for energy and quasi-momentum eigenvalues is of order $\mathcal{O}(L^{-2})$.

Furthermore, we present a unifying framework for NLIEs, distinguishing between versions with singular and regular kernels. We provide a compact derivation of NLIE with a singular kernel, followed by an equivalent set with a regular kernel. We address the stability issues in numerical treatments and offer solutions to achieve high-accuracy results, validating our approach for system sizes ranging from $L = 2$ to $L = 10^{24}$.

Our findings not only validate the ODE/IQFT approach for finite system sizes but also enhance the understanding of NLIEs in the context of the staggered six-vertex model. We hope the insights gained from this study have significant implications for resolving the spectral problem of other lattice systems with emergent non-compact degrees of freedom and provide a foundation for future research in this domain.

1 Introduction

The study of two-dimensional (2D) integrable lattice systems, such as the Ising model, the six-vertex model, and the eight-vertex model, alongside their associated one-dimensional (1D) integrable quantum spin chains, has significantly shaped our understanding of universality and critical phenomena. These models continue to be pivotal in the exploration of correlation functions both in and out of equilibrium [1–3], and in the study of quantum entanglement [4].

A basic yet fundamental example is the homogeneous six-vertex model, particularly when the anisotropy parameter q is unimodular ($|q| = 1$). In the scaling limit, this model is described by a compact massless 1+1 dimensional boson field. However, more intriguing behaviors emerge in the integrable, inhomogeneous six-vertex model introduced by Baxter [5]. Specifically, when staggered inhomogeneities are introduced, the model exhibits two distinct types of universal behavior depending on the value of q [6].

Jacobsen and Saleur [6, 7] revealed that the theory possesses a continuous spectrum of scaling dimensions. A significant conjecture by Ikhlef, Jacobsen, and Saleur [8] proposed that the staggered lattice model realizes the Euclidean black hole non-linear sigma model (NLSM) in the scaling limit, connecting it to works on black hole CFTs

[9–14]. This conjecture was confirmed and further elaborated by Bazhanov, Kotousov, Koval, and Lukyanov [15, 16] and [17] through the ODE/IQFT approach, establishing the scaling limit is related to the 2D Euclidean/Lorentzian black hole CFTs. The lattice analysis has been essential in resolving the spectral problem for the 2D Euclidean black hole field theory, including determining the density of states for the continuous spectrum [16].

Linear integral equations for density functions of Bethe roots for models with emerging non-compact degrees of freedom have been used by Ikhlef, Jacobsen, and Saleur [8, 18], as well as by Frahm and Martins [19, 20]. These equations are derived for density functions defined in the thermodynamic limit. Results obtained from these density functions, calculated either numerically or, under certain conditions, analytically, yield bulk properties. When finite “Fermi points” are considered, this approach allows for Sommerfeld-like computations of finite size quantities. In cases where the distributions of roots span the entire real axis, the Wiener-Hopf technique may be applied [8]. Our paper addresses the case of strictly finite size systems.

For finite systems, non-linear integral equations (NLIEs) based on the Bethe Ansatz have been instrumental. Candu and Ikhlef [21] as well as Frahm and Seel [22], were the first to derive NLIEs for the staggered six-vertex model, significantly contributing to the understanding and solution of these equations. In this paper, we present a unifying framework for NLIEs, particularly useful for high-accuracy calculations in the context of the staggered six-vertex model.

We study the spectral properties of the staggered six-vertex model with \mathbb{Z}_2 symmetry. We are primarily interested in the accuracy of the results based on the ODE/IQFT correspondence in the asymptotic regime of large system sizes, and in finding the optimal approach based on NLIE for studying the staggered six-vertex model. We found that the quantization conditions for low-lying primary states obtained in [8] and improved and extended to descendant states in the works of Bazhanov et al. [15–17, 23], are impressively accurate for a wide range of sizes. In the anisotropy parameter range $\pi/4 < \gamma < \pi/2$, the difference between NLIE and ODE/IQFT results for energy and quasi-momentum eigenvalues vanishes in the scaling limit as $\mathcal{O}(L^{-2})$.

We also analyze different versions of NLIE, noting that while some have singular kernels, others have regular kernels. We present a compact derivation of the NLIE with singular kernel from which the relationship to the other versions is understood. By rearranging terms, we derive an equivalent set of NLIE with regular kernel. We explain the stability issues in the numerical iterative treatment of these equations and provide solutions with high numerical accuracy. We performed calculations for lattice sizes ranging from $L = 2$ to $L = 10^{24}$, showing excellent agreement with ODE/IQFT results.

The structure of this paper is as follows: Section 2 reviews the fundamental aspects of the six-vertex model and its staggered variant. Section 3 presents the derivation of our first version of NLIE with a singular integral kernel for the lowest-lying states of the model. In Section 4, we derive an equivalent version with a regular kernel and present numerical results for various system sizes, comparing these results to those obtained using the ODE/IQFT approach. Section 5 presents the analytic derivation of the main logarithmic term in the spectrum using the singular kernel version of our NLIEs without resorting to Wiener-Hopf techniques. Section 6 addresses necessary modifications of the NLIE for dealing with non-primary states. Finally, in Section 7, we summarize our results, suggest directions for future research, and provide more technical information in the Appendix.

2 The staggered six-vertex model: definition and eigenvalue equation

We study the six-vertex model with standard R-matrix acting on the tensor product of two 2-dimensional vector spaces by following in this section largely the notation of [21]. The only non-zero elements of R in the standard basis, $|++\rangle, |+-\rangle, |-+\rangle, |--\rangle$, are

$$R_{++}^{++}(u) = R_{--}^{--}(u) = a(u), \quad R_{+-}^{+-}(u) = R_{-+}^{+-}(u) = b(u), \quad R_{+-}^{+-}(u) = R_{-+}^{+-}(u) = c(u). \quad (1)$$

where $a(u) = \sin(\gamma - u)$, $b(u) = \sin(u)$, $c(u) = \sin(\gamma)$, u is referred to as the spectral parameter, and γ is the anisotropy parameter. A suitable product of R-matrices with same spectral parameter u yields the commuting family of row-to-

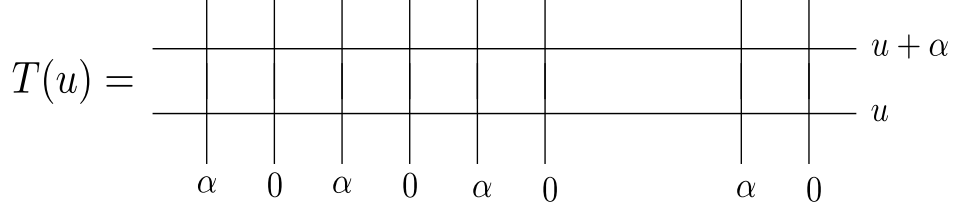


Figure 1: Depiction of the double row transfer matrix of the staggered 6-vertex model.

row transfer matrices $T(u)$ whose logarithmic derivative at $u = 0$ is the Hamiltonian of the $S = 1/2$ XXZ quantum spin chain. In our paper we use periodic boundary conditions.

The model allows for generalizations keeping its integrability [5]. A modest generalization is given by the staggering of the spectral parameter from column to column [6]. The alternating product of $R(u)$ and $R(u - \alpha)$, with fixed parameter α , in dependence on u still yields a commuting family of transfer matrices, which for simplicity again will be called $T(u)$.

The logarithmic derivative of $T(u)$ at $u = 0$ resp. at $u = \alpha$ yields a sum of locally acting terms, unfortunately without particular symmetries. However, the sum of these operators, i.e. the logarithmic derivative of the product $T(u)T(u + \alpha)$ at $u = 0$ exhibits \mathcal{CP} and \mathcal{T} invariance [16]. This follows among other things from unitarity and the standard initial condition of the R-matrix. Fig. 1 shows an illustration of the construction principle on the square lattice. To each vertical line a spectral parameter 0 or α is assigned and to the horizontal lines u or $u + \alpha$. Each vertex is associated with an R-matrix whose argument is given by the difference of the spectral parameters on the intersecting horizontal and vertical lines. The lower row corresponds to $T(u)$, the upper row to $T(u + \alpha)$. For general values of α the double row transfer matrix with periodic boundary conditions is invariant under a translation by 2 lattice sites. For $\alpha = \pi/2$ an invariance under a translation by 1 lattice site is restored, and also, the system shows a \mathbb{Z}_2 symmetry [16]. Note that generalizations of staggered six-vertex models with \mathbb{Z}_r symmetry have been studied in [23, 24].

The quantum Hamiltonian of the spin- $\frac{1}{2}$ chain of length $2L$ associated with the double-row transfer matrix is expressed in terms of Pauli matrices which for the case $\alpha = \pi/2$ has explicit form

$$\begin{aligned} H &= \frac{1}{2} \sin(2\gamma) \cdot \partial_u \log [T(u)T(u + \pi/2)] \big|_{u=0} \\ &= \sum_{j=1}^{2L} \left[-\frac{1}{2} \vec{\sigma}_j \vec{\sigma}_{j+2} + \sin^2(\gamma) \sigma_j^z \sigma_{j+1}^z - \frac{i}{2} \sin(\gamma) \left(\sigma_{j-1}^z - \sigma_{j+2}^z \right) \left(\sigma_j^x \sigma_{j+1}^x + \sigma_j^y \sigma_{j+1}^y \right) \right] + L \cos(2\gamma). \end{aligned} \quad (2)$$

In this paper, we restrict ourselves to the regime of the anisotropy parameter $\pi/4 < \gamma < \pi/2$.

As is well known, each eigenvalue Λ of the transfer matrix $T(u)$ of the six-vertex model satisfies the T - q equation. This reads

$$\Lambda(z)q(z) = \Phi(z - i\gamma)q(z + 2i\gamma) + \Phi(z + i\gamma)q(z - 2i\gamma), \quad (3)$$

after a transformation of the variable $u = -(i/2)z + \gamma/2$ to the argument z . The factor $\Phi(z - i\gamma)$ is the L -th power of $a(u)a(u - \pi/2) = \sin(\gamma - u) \sin(\gamma - u + \pi/2) = (i/2) \sinh(z - i\gamma)$, and $\Phi(z + i\gamma)$ is the L -th power of $b(u)b(u - \pi/2) = \sin(u) \sin(u - \pi/2) = (i/2) \sinh(z + i\gamma)$. Hence

$$\Phi(z) := \sinh^L(z), \quad q(z) := \prod_{j=1}^N \sinh \frac{1}{2}(z - z_j), \quad (4)$$

where we have dropped the factor $(i/2)^L$ in Φ . Whenever necessary this factor has to be retrieved. However, in the following we will be interested in logarithmic derivatives and ratios of the eigenvalue functions.

The Bethe ansatz roots (or rapidities) z_j , $j = 1, \dots, N$, $0 \leq N \leq L$, have to satisfy the Bethe ansatz equations:

$$a(z_j) = -1, \quad j = 1, \dots, N, \quad (5)$$

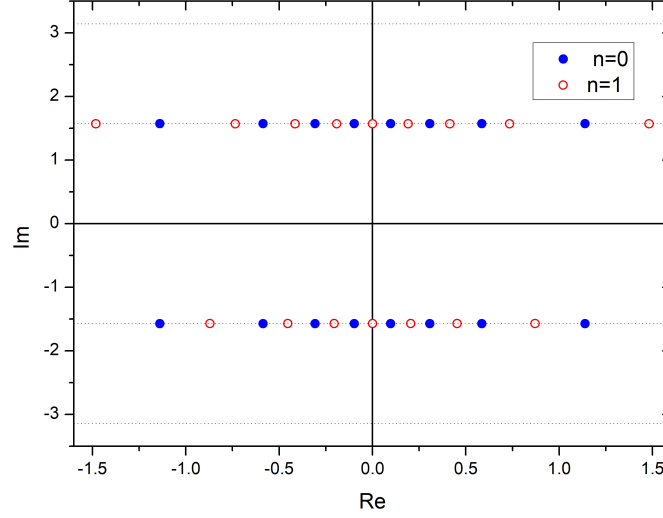


Figure 2: Depiction of the location of all zeros of $q(z)$ in the complex plane for $L = 16$ and $\gamma = 0.8$. Disks refer to the ground state ($n = 0$) and circles to the first excited state ($n = 1$).

where the function $a(z)$ – not to be confused with the Boltzmann weight appearing in (1) – is defined as

$$a(z) := \frac{\Phi(z + i\gamma)q(z - 2i\gamma)}{\Phi(z - i\gamma)q(z + 2i\gamma)}. \quad (6)$$

For the largest eigenvalue and a large class of next-leading eigenvalues the total number of roots is equal to L with the distribution of the roots along the horizontal axes through $\pm i\pi/2$. Here we consider $L/2 \pm n$ roots located on the upper/lower axis with L typically much larger than n . See Fig. 2 for anisotropy parameter $\gamma = 0.8$ for distributions of roots for $L = 16$ with $n = 0$ and 1. The truly largest eigenvalue Λ , corresponding to the ground state energy of the quantum chain, is given by the case $n = 0$.

In the next sections we restrict ourselves to the low-lying states just described. The CFT descendants to these states are considered in Sect. 6. More general cases, primary states corresponding to distributions of roots with holes and descendants to these, will be published in separate work.

3 Non-linear integral equations: singular kernel version

The eigenvalues $\Lambda(z)$ of $T(z)$ are analytic functions of the spectral parameter u . In this paper, we use this analyticity and adopt a method in analogy to the approach in [25], see also [26–30], to determine the eigenvalues by a finite set of non-linear integral equations (NLIE) and valid for arbitrary (even) system size. This approach also allows for taking the limit $L \rightarrow \infty$ analytically. The central object is the function $a(z)$ (6) in the complex plane. It has zeros of order L at $-i\gamma, (\pi - \gamma)i$ and poles of order L at $+i\gamma, (\pi + \gamma)i$. As we will see shortly, it will be useful to consider $a(z)$ and its

reciprocal on the horizontal axes through the points of high order zeros and poles:

$$a_1(x) := \frac{1}{a(x+i\gamma)} = \frac{\Phi(x)}{\Phi(x+2i\gamma)} \frac{q(x+3i\gamma)}{q(x-i\gamma)}, \quad (7)$$

$$a_2(x) := a(x+i\pi-i\gamma) = \frac{\Phi(x)}{\Phi(x-2i\gamma)} \frac{q(x+i\pi-3i\gamma)}{q(x+i\pi+i\gamma)}, \quad (8)$$

$$a_3(x) := a(x-i\gamma) = \frac{\Phi(x)}{\Phi(x-2i\gamma)} \frac{q(x-3i\gamma)}{q(x+i\gamma)}, \quad (9)$$

$$a_4(x) := \frac{1}{a(x+i\pi+i\gamma)} = \frac{\Phi(x)}{\Phi(x+2i\gamma)} \frac{q(x+i\pi+3i\gamma)}{q(x+i\pi-i\gamma)}, \quad (10)$$

where the explicit factorization in terms of $\Phi(z)$ and $q(z)$ is shown on the right. These functions by themselves do not define a closed system of functional equations. This is achieved by introducing the additional set of closely related functions

$$A_i(z) := 1 + a_i(z). \quad (11)$$

By use of the functional equation (3) these functions can be written in terms of $\Lambda(z)$ as follows

$$A_1(x) = \frac{1}{\Phi(x+2i\gamma)} \frac{q(x+i\gamma)}{q(x-i\gamma)} \Lambda(x+i\gamma), \quad (12)$$

$$A_2(x) = \frac{1}{\Phi(x-2i\gamma)} \frac{q(x+i\pi-i\gamma)}{q(x+i\pi+i\gamma)} \Lambda(x+i\pi-i\gamma), \quad (13)$$

$$A_3(x) = \frac{1}{\Phi(x-2i\gamma)} \frac{q(x-i\gamma)}{q(x+i\gamma)} \Lambda(x-i\gamma), \quad (14)$$

$$A_4(x) = \frac{1}{\Phi(x+2i\gamma)} \frac{q(x+i\pi+i\gamma)}{q(x+i\pi-i\gamma)} \Lambda(x+i\pi+i\gamma). \quad (15)$$

The key of our approach is the identification of analyticity domains in which the functions $q(z)$ and $\Lambda(z)$ are free of zeros, i.e. domains where these functions are analytic and non-zero (ANZ). We find two such analyticity strips for each function modulo $2\pi i$ -periodicity. Hence there exist four Fourier transform expressions for all q and Λ data on the right hand sides of (7)-(10) and (12)-(15). This will allow for the derivation of a closed set of integral equations for the functions a_i and for integral expressions for the eigenvalue function.

By periodicity we can restrict our attention to fundamental regions of height 2π in the complex plane. These are taken slightly differently for the functions $q(z)$ and $\Lambda(z)$: $-\frac{1}{2}\pi < \text{Im}(z) < \frac{3}{2}\pi$ and $0 < \text{Im}(z) < 2\pi$, see Fig. 3 for parameters $L = 16$ and $\gamma = 0.8$. In the same figure, the zeros of $\Lambda(z)$ are also shown. An index I resp. II labels the strips where no zeros are present. The ANZ strips for $q(z)$ are (I) $-\frac{1}{2}\pi < \text{Im}(z) < \frac{1}{2}\pi$ and (II) $\frac{1}{2}\pi < \text{Im}(z) < \frac{3}{2}\pi$. For $\Lambda(z)$ the ANZ strips are (I) $-\pi < \text{Im}(z) < 0$ and (II) $0 < \text{Im}(z) < \pi$ (actually a little narrower due to the deviations of zeros from the straight lines).

First we observe from (7)-(10) and (12)-(15) that the functions a_i take very small values for argument x in the neighbourhood of 0 and have simple asymptotes

$$a_i(\pm\infty) = 1, \quad A_i(\pm\infty) = 1 + a_i(\pm\infty) = 2, \quad i = 1, \dots, 4. \quad (16)$$

Their continuous logarithms for argument x along the real axis have well defined finite asymptotic values for $-\infty$ and $+\infty$. Note that in general these asymptotic values need not be the same. Notably for the functions $\log a_i(x)$ we observe an increase or decrease of the imaginary part by multiples of 2π . This value, i.e. the winding of $a_i(x)$ around 0 for x from $-\infty$ to $+\infty$, serves as a strict quantization condition for the eigenvalues. Of course, the logarithmic derivative of all functions can be Fourier-transformed and equations (7)-(10) and (12)-(15) turn into eight linear relations for the Fourier transforms. We like to note that the logarithmic derivatives of q and Λ have non-zero and different asymptotic

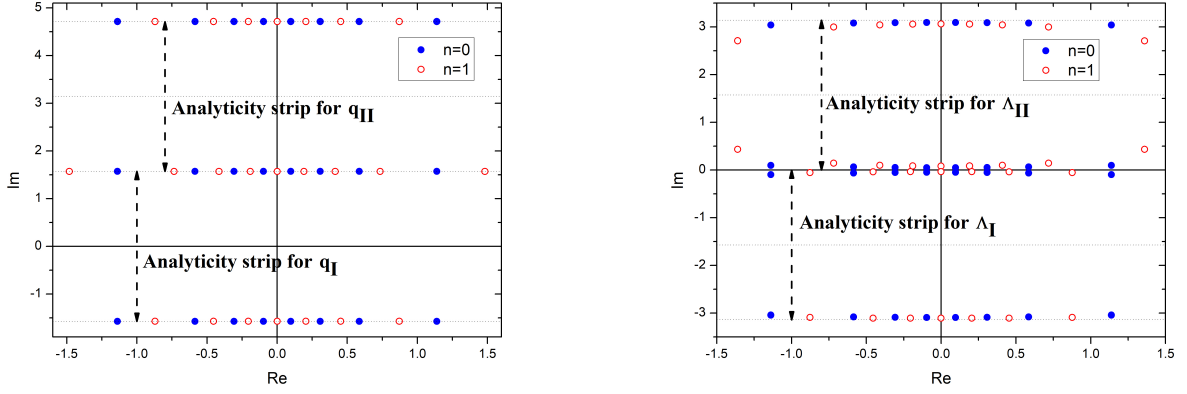


Figure 3: Depiction of the location of all zeros in the complex plane for a) the function $q(z)$ and b) the eigenvalue function $\Lambda(z)$. We use parameters $L = 16$ and $\gamma = 0.8$. Note that the functions are $2\pi i$ periodic. Disks refer to the ground state ($n = 0$) and circles to the first excited state ($n = 1$). The zeros of $q(z)$ lie precisely on straight lines, the zeros of $\Lambda(z)$ are close to \mathbb{R} and to $\mathbb{R} \pm i\pi$, but deviate from them. The strips of the complex plane that are free of zeros of $q(z)$ and $\Lambda(z)$ allow for the Fourier transform of the logarithmic derivatives of the functions. We refer to these Fourier representations in different strips by indices I and II to indicate which analyticity strip is used. Note that strips I and II are different for $q(z)$ and $\Lambda(z)$.

values for the real part of the argument to $-\infty$ and $+\infty$. Therefore strictly speaking we should work with Fourier transforms of second derivatives of the logarithms of all involved functions.

Next we fix the definitions of the Fourier transform $\mathfrak{F}_k\{f\}$ (and its inverse) of a complex function $f(z)$ which is analytic in a certain strip and decays sufficiently fast. The Fourier transform pair is

$$\mathfrak{F}_k\{f\} := \frac{1}{2\pi} \int_{\mathcal{C}} f(x) e^{-ikx} dx, \quad f(x) = \int_{-\infty}^{\infty} \mathfrak{F}_k\{f\} e^{ikx} dk. \quad (17)$$

where the integration path \mathcal{C} is the real axis or has to lie in the appropriate analyticity strip of the functions $q(z)$ and $\Lambda(z)$. Note that the Fourier transforms of (the derivative of) $\log q(z)$ in strips I and II differ. For that reason we index these functions by I and II and have to consider them as different. The same remark applies to the function $\Lambda(z)$. Note that the inverse Fourier transforms with k -integrals along the real axis have different convergence regions for different indices I and II: these are the above identified ANZ strips I and II.

For multiplicative relations like

$$f(x) = g(x + i\alpha)/h(x + i\beta),$$

with shifts leaving the argument in the analyticity strip of the respective function, the Fourier transform of the logarithmic derivative yields

$$\mathfrak{F}_k\{(\log f)'\} = e^{-\alpha k} \mathfrak{F}_k\{(\log g)'\} - e^{-\beta k} \mathfrak{F}_k\{(\log h)'\}.$$

This relation also holds for the Fourier transform of the second logarithmic derivative.

The eight multiplicative relations (7)-(10) and (12)-(15) yield eight linear equations for the Fourier transforms of the logarithmic derivatives of the functions $a_1, a_2, a_3, a_4, A_1, A_2, A_3, A_4, q_I, q_{II}, \Lambda_I$ and Λ_{II} . These can be solved uniquely for $a_1, a_2, a_3, a_4, q_I, q_{II}, \Lambda_I$ and Λ_{II} in terms of A_1, A_2, A_3, A_4 with certain k -dependent factors. The inverse Fourier transform consists of explicit functions and in addition of convolution integrals of explicit functions with $\log A_i$ functions. Details can be found in the appendix.

We apply this strategy, do the inverse Fourier transform and obtain integral equations first for the differentiated logarithms of a_i in terms of those for A_i . We finally integrate with respect to x , identify the integration constants and obtain, the following compact form of the NLIE of the staggered 6-vertex model:

$$a = d + K * A, \quad (18)$$

where

$$a(x) = \begin{pmatrix} \log a_1(x) \\ \log a_2(x) \\ \log a_3(x) \\ \log a_4(x) \end{pmatrix}, \quad A(x) = \begin{pmatrix} \log A_1(x) \\ \log A_2(x) \\ \log A_3(x) \\ \log A_4(x) \end{pmatrix}, \quad d(x) = L \log(\tanh(\frac{1}{2}gx)) \cdot \begin{pmatrix} 1 \\ 1 \\ 1 \\ 1 \end{pmatrix}, \quad g := \frac{\pi}{\pi - 2\gamma}, \quad (19)$$

where $d(x)$ is the driving resp. source term. The notation $g * f$ denotes the convolution of the functions g and f ,

$$(g * f)(x) = \frac{1}{2\pi} \int_{-\infty}^{\infty} g(x-y)f(y)dy, \quad (20)$$

where we introduced the prefactor $1/2\pi$ for convenience in some situations. This set of integral equations holds for any imbalance n of the number of roots on the axes with imaginary parts $\pm\pi/2$.

The kernel has the following block structure

$$K = \begin{pmatrix} \sigma_1 & \sigma_2 \\ \sigma_2^\dagger & \sigma_1^T \end{pmatrix}, \quad (\dagger \text{ interchanges diagonal elements}). \quad (21)$$

where in Fourier representation we have

$$\sigma_1 = \frac{\cosh((\pi - 3\gamma)k)}{2 \sinh(\gamma k) \sinh((\pi - 2\gamma)k)} \begin{pmatrix} -1 & e^{(\pi - 2\gamma)k} \\ e^{(2\gamma - \pi)k} & -1 \end{pmatrix}, \quad (22)$$

$$\sigma_2 = \frac{\cosh(\gamma k)}{2 \sinh(\gamma k) \sinh((\pi - 2\gamma)k)} \begin{pmatrix} -e^{(\pi - 2\gamma)k} & 1 \\ 1 & -e^{(2\gamma - \pi)k} \end{pmatrix}. \quad (23)$$

The kernel is singular as it has a pole of second order at $k = 0$. The inverse Fourier transform involves functions that do not decay at large distances, they increase linearly!

At first glance these integral equations look useless and possibly ill-defined. The right way to look at them is that the left-hand side is well defined and via the integral equations imposes a condition on the functions on the right-hand side in order for the convolution integral to exist. This applies to the solutions to the integral equations. Unfortunately, it does not apply to all functions generated in an iterative application of the equations when starting with some initial data.

Of course, when using the above set of integral equations we have to say how the inverse Fourier transform of (21) is precisely defined. This we treat in section 5 and in the appendix. In section 4 we will derive from (18) an alternative equivalent set of NLIE however with regular kernel. Before doing so we like to present some results to illustrate some properties of the functions and to substantiate claims made above.

In Fig. 4 we show graphs of the real and imaginary parts of the functions $\log a_i - d$ and $\log A_i = \log(1 + a_i)$ for the true ground state solution and system size $L = 10^{10}$, $\gamma = 0.8$. Reallocating one root from one axis to the other ($n = \pm 1$) has a solution that is shown in Fig. 5. Note that the changes in comparison to the ground state are minor for the functions $\log A_i$, but there are huge changes in the $\log a_i$ functions. These functions no longer show equal asymptotics for argument to $-\infty$ and $+\infty$. Instead they show a winding of the trajectories of the functions $a_i(x)$ around 0: the asymptotics of $\text{Im} \log a_i(x)$ change by $2\pi i$ from $-\infty$ and $+\infty$ with almost linear dependence on the argument x in the interval $[-(\log L)/g, +(\log L)/g]$, see also the reasoning following (43).

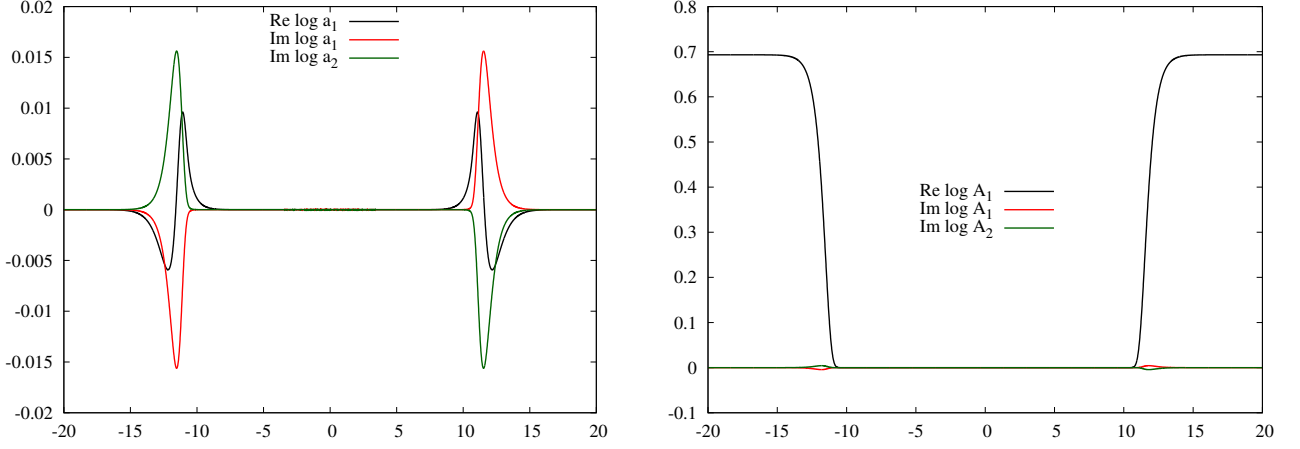


Figure 4: The true ground state of the system with $L/2$ roots located on the upper as well as on the lower axis: a) Depiction of real and imaginary parts of the functions $\log a_j - d$ with $j = 1, 2, 3, 4$. The real parts are identical for all j , the imaginary parts are identical for $j = 1, 3$ ($j = 2, 4$). Similar depiction of the functions $\log A_j = \log(1 + a_j)$. We use parameters $L = 10^{10}$ and $\gamma = 0.8$.

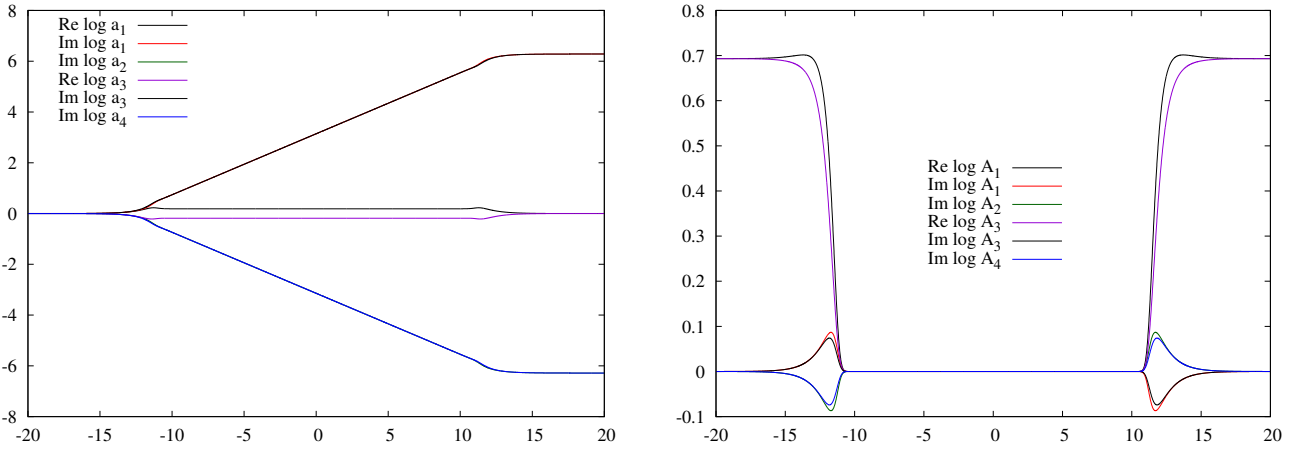


Figure 5: The first excited state ($n = 1$) of the system with $L/2 + 1$ roots located on the upper axis and $L/2 - 1$ roots on the lower axis: a) Depiction of real and imaginary parts of the functions $\log a_i - d$ with $i = 1, 2, 3, 4$. The real parts for $i = 1, 2$ ($i = 3, 4$) are identical and shown by a black (violet) line. The imaginary parts for $i = 1$ and 3 ($i = 2$ and 4) are similar and shown by red and black (green and blue) lines. b) Similar depiction of the functions $\log A_i = \log(1 + a_i)$.

4 Non-linear integral equations: regular kernel version

There are many alternative ways to write equation (18), i.e. with not only $\log A_i$ on the right hand side, but also with $\log a_i - d$ functions. We found that the following one is valid and useful

$$a = d + K_r * (a - d - 2A) \quad \text{with} \quad K_r := \frac{K}{K - 2}. \quad (24)$$

The equivalence to (18) is shown by straightforward “algebraic” rewriting. The kernel K_r has a block structure similar to K

$$K_r = \begin{pmatrix} \kappa_1 & \kappa_2 \\ \kappa_2^\dagger & \kappa_1^T \end{pmatrix}, \quad (\dagger \text{ interchanges diagonal elements}). \quad (25)$$

but unlike K the entries are regular functions at $k = 0$

$$\kappa_1(k) = \frac{\sinh((\pi - 2\gamma)k)}{2 \sinh(\pi k)} \begin{pmatrix} 1 & -e^{(\pi - 2\gamma)k} \\ -e^{(2\gamma - \pi)k} & 1 \end{pmatrix}, \quad \kappa_2(k) = \frac{\sinh(2\gamma k)}{2 \sinh(\pi k)} \begin{pmatrix} e^{(\pi - 2\gamma)k} & -1 \\ -1 & e^{(2\gamma - \pi)k} \end{pmatrix}. \quad (26)$$

The inverse Fourier transform yields (with a slight abuse of notation: $\kappa_j(k)$ is the Fourier transform of $\kappa_j(x)$)

$$\kappa_1(x) = \begin{pmatrix} \sigma(x) & -\sigma(x - (\pi - 2\gamma)i) \\ -\sigma(x + (\pi - 2\gamma)i) & \sigma(x) \end{pmatrix}, \quad \kappa_2(x) = \begin{pmatrix} -\sigma(x + 2\gamma i + i\epsilon) & \sigma(x - \pi i) \\ \sigma(x + \pi i) & -\sigma(x - 2\gamma i - i\epsilon) \end{pmatrix}, \quad (27)$$

and

$$\sigma(x) := \frac{i}{2} \left(\frac{1}{1 - e^{-x - 2\gamma i}} - \frac{1}{1 - e^{-x + 2\gamma i}} \right) = \frac{\sin 2\gamma}{4 \sinh(x/2 + \gamma i) \sinh(x/2 - \gamma i)}. \quad (28)$$

Generally, equation (24) is of a type that allows for a direct iterative method (like in [25, 31]) to obtain, for arbitrary lattice size L and anisotropy γ , a numerical solution of high accuracy. Among other things, for doing efficient computations of the convolution integrals we use fast Fourier transform (FFT). The first question that arises when looking at (24) is how it is possible that all singularities have disappeared and no problems – possibly in different clothing – appear? The convolution integrals are indeed well-defined. The right hand side of (24) viewed as an operator has most eigenvalues of absolute value below 1, except one eigenvalue at $k = 0$ which is exactly +1. The corresponding eigenvector, however, does not realize an instability to convergence in the iterative numerical calculations. This is largely prohibited by the bulk behaviour of the functions in the interval $[-(\log L)/g, +(\log L)/g]$. Next to mention is the peculiar factor 2 in the combination $a - d - 2A$. By this, the functions $a - 2A$, or in extended notation $\log a_i(x) - 2 \log A_i(x)$, have very quickly decaying asymptotics for $x \rightarrow \pm\infty$. And last, the combination $a - d$ has numerically small values as d is the bulk behaviour of a .

Here a note on the relation of our integral equations to those used by [21, 22] is in order. In [21] the NLIE of the form (18) is used, the leading singular behaviour of the kernel is extracted resulting in additional source terms. The so treated NLIE in the scaling limit is then solved numerically. The work [22] uses a different version of NLIE of course related to (18) resp. [21]. The NLIEs of [22] can be obtained with functions on contours similar to (7)-(10) however without taking the reciprocal of the function a in the definition of a_1 and a_3 . Following the steps presented above we arrive at NLIEs of the form (18) for the modified functions \tilde{a}_j and $\tilde{A}_j = 1 + \tilde{a}_j$ with a different kernel which appears to be regular. Technically, in [22] the NLIEs are presented in closed contour formulation.

We find that the form (24) is highly useful for treating unprecedented ranges of values for L and in principle any lattice size we want with high numerical accuracy. In this paper we limit our numerics to values of L between 2 and 10^{24} . For efficient numerics we use the Fast Fourier Transform for calculating the convolution integrals. To this end the eqns. (24) need the application of certain subtraction terms to render the functions entering the convolutions Fourier transformable. This will be treated in the next paragraph. A final remark on the two different versions of the

NLIEs that we deal with: the “singular” version of the NLIE (18) is not at all useless. It is important to note that the singular nature of the kernel is closely connected to the emergence of a continuous spectrum in the continuum limit of the model as discussed by Candu and Ikhlef in [21]. It will allow for an analytic derivation of at least the leading logarithmic terms in the large size asymptotics, see Sect. 5.

Note that (24) like (18) holds for any imbalance n of the number of roots on the axes with imaginary parts $\pm\pi/2$. For $n = 0$ the solution functions have simple asymptotics as shown in Fig. 4. However, shifting n BA roots from one axis to the other one yields a winding of the $\log a_i(x)$ functions: $\log a_i(\infty) - \log a_i(-\infty) = \pm n 2\pi i$. Interestingly, (24) holds for any n , but does not contain any n dependent term. The convolution integral in (24) is well-defined for any n , but does not allow for an application of the Fourier transform, because of the different asymptotes for non-zero n . This problem is cured by subtracting and adding analytic functions w and \tilde{w} with the property $w = K_r * \tilde{w}$, such that

$$a = d + K_r * (a - d - 2A) = d + n w + K_r * (a - d - n \tilde{w} - 2A), \quad (29)$$

and $a - n \tilde{w}$ has same asymptotical values at $-\infty$ and at $+\infty$. This is achieved by for instance the functions

$$w(x) = \begin{pmatrix} w_1(x) \\ w_2(x) \\ w_3(x) \\ w_4(x) \end{pmatrix}, \quad \tilde{w}(x) = 2 \log \tanh \left(\frac{g}{2} x + i \frac{\pi}{4} \right) \cdot \begin{pmatrix} +1 \\ -1 \\ +1 \\ -1 \end{pmatrix}, \quad (30)$$

and

$$w_1(x) = -w_4(x) := \log \tanh \frac{1}{2} \left(x + i \left(\frac{\pi}{2} - \gamma \right) \right) + \log \tanh \frac{1}{2} \left(x + i \left(3\gamma - \frac{\pi}{2} \right) \right), \quad (31)$$

$$w_2(x) = -w_3(x) := \log \tanh \frac{1}{2} \left(x - i \left(\frac{\pi}{2} - \gamma \right) \right) + \log \tanh \frac{1}{2} \left(x - i \left(3\gamma - \frac{\pi}{2} \right) \right). \quad (32)$$

In our numerical calculations we have used variations of these functions like convolutions of the w_j, \tilde{w}_j with functions that increase linearly in the interval $[-(\log L)/g, +(\log L)/g]$ such that the modified w_j, \tilde{w}_j are still smooth, but mimic the behaviour of the functions $\log a_j$. This leads to a slight improvement in the numerical accuracy.

Eq. (29) is the final version of NLIE that we use for the numerical treatment of the low-lying energy states as long as the distributions of the zeros of q , i.e. the Bethe roots, and of the zeros of the eigenvalue function Λ are as we described above.

We now use the number n , i.e. the winding number of the functions a_i , as the fundamental variable. The quasi-momentum, see [8] and (37), is a derived property and does not play a central role in our treatment.

Within the presented treatment it is also possible to obtain a simple expression for the energy in terms of the auxiliary functions $\log A_i$. For details see the Appendix. Here we give the integral expression for the relevant combination of the eigenvalue functions which splits into a pure bulk and a finite size part

$$\log[\Lambda(x - i\gamma)\Lambda(x + i(\pi - \gamma))] = L \cdot \lambda_0(x) + \kappa * [\log A_1 + \log A_2 + \log A_3 + \log A_4]. \quad (33)$$

The kernel function κ is given by

$$\kappa(x) = -i \frac{g}{\sinh(gx)}. \quad (34)$$

The energy is calculated from the derivative at $x = 0$

$$E = \sin(2\gamma) i \frac{d}{dx} \log[\Lambda(x - i\gamma)\Lambda(x + i(\pi - \gamma))] \quad (35)$$

$$= Le_0 - \frac{\sin(2\gamma)}{2\pi} \int_{-\infty}^{\infty} dx \frac{g^2 \cosh gx}{(\sinh gx)^2} [\log A_1(x) + \log A_2(x) + \log A_3(x) + \log A_4(x)], \quad (36)$$

where e_0 is the bulk energy obtained from $\lambda_0(x)$, and we remind of the definition of g in (19).

The so-called quasi-momentum K [8] is the logarithm of the quasi-shift operator

$$\tilde{\tau} := T(\pi/2)T^{-1}(0). \quad (37)$$

The eigenvalue for a given state is obtained from the function

$$K(x) := \log \frac{\Lambda(x + i(\pi - \gamma))}{\Lambda(x - i\gamma)} = \tilde{\mathbf{k}} * [\log A_1 - \log A_2 + \log A_3 - \log A_4], \quad \tilde{\mathbf{k}}(x) = ig \coth(gx), \quad (38)$$

at argument $x = 0$

$$K = K(0) = \frac{g}{2\pi i} \int_{-\infty}^{\infty} dx \coth gx [\log A_1(x) - \log A_2(x) + \log A_3(x) - \log A_4(x)]. \quad (39)$$

As the model is critical the spectrum of the low-lying excitations can be described within the framework of CFT. The finite size parts were calculated previously by different approaches [8, 15, 21, 22]

$$E(L) = Le_0 + \frac{2\pi}{L} v_F \left(-\frac{1}{6} + \frac{\gamma}{2\pi} m^2 + \frac{\pi}{2\gamma} w^2 + \frac{2g\gamma}{\pi} s^2 + N \right), \quad v_F = g \sin(2\gamma), \quad (40)$$

which means that the (effective) central charge is $c = 2$. Here v_F is the Fermi velocity and m and w are integers identical to the magnetization (number of flipped spins) and to the imbalance of the root distributions between left and right, N is the integer labeling the levels of the conformal tower. The case we studied above corresponds to $m = w = N = 0$.

The energy contributions due to the parameter s originate from rather remarkable logarithmic finite-size corrections as a consequence of the reallocation of the number n of BA-roots from one axis to the other. The Wiener-Hopf analysis in [8] resulted in

$$s \simeq \frac{\pi n}{2 \log L} \quad \text{for large } L, \quad n = 0, \pm 1, \pm 2, \dots \quad (41)$$

In the thermodynamical limit this term signifies a non-compact degree of freedom as the discretization of s is on the logarithmic scale $1/\log(L)$ and to be considered a continuous parameter.

The result for the quasi-momentum in terms of s is

$$K = 4g\gamma s. \quad (42)$$

To illustrate, we obtain the result (40,41) for the energy and the quasi-momentum in Sect. 5 by simple manipulations starting from (18) without solving any NLIEs, not to mention using Wiener-Hopf techniques.

In Fig. 6 we show the results of our calculations for various values of n and system sizes from $L = 2$ to $L = 10^{24}$. The data obtained for the energy resp. the quasi-momentum are used to identify the parameter s from (40) resp. (42). We plot n/s as function of L and see clearly the asymptotic behaviour (41).

The finite, i.e. next order term to (41) resp. to the density of states $(\partial n / \partial s)$ was obtained in [21, 22] by numerical calculations based on the NLIEs used by the authors. The most accurate analytical results for the asymptotics of s , in the form of a quantization condition, are given in [8] and especially in [15] by use of the ODE/IQFT correspondence.

In Fig. 7, we compare energy and quasi-momentum for different values of n and various system sizes obtained from a numerical solution of (24) with the results of [15], see also (B.1)-(B.3) in the appendix. The values of the parameters used in the plot are $\gamma = 0.8$ and $n = 0, 1, 2, 3$. Our NLIE are exact for all (even) lattice sizes even for the smallest value $L = 2$. The quantization condition [15] has been derived for large sizes, but interestingly it is rather accurate also for small lattice sizes. The difference of the two approaches is best fitted by an order $\mathcal{O}(L^{-2})$ ansatz (for $\pi/4 < \gamma < \pi/2$ where we carried out our numerical calculations).

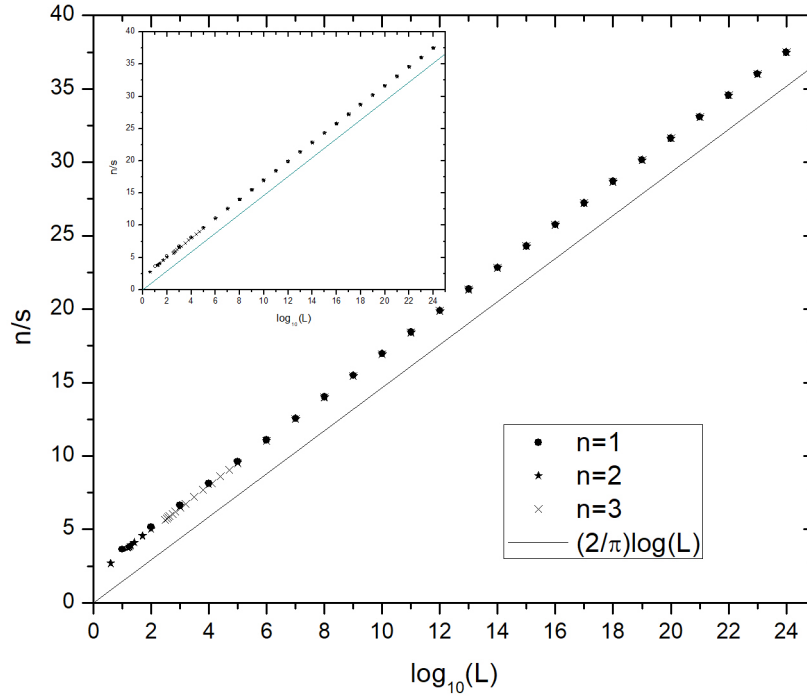


Figure 6: Plot of the ratio n/s against system size L with quasi-momentum parameter s obtained from calculations of energies E_{NLIE} (main panel) and quasi-momenta K_{NLIE} (inset) by use of the NLIE (29). The continuous line corresponds to the asymptotic behavior (41). The symbols lie above this line by an offset $\log L_0$ defining the non-universal length scale L_0 . The data have been obtained for parameters $\gamma = 0.8$ and $n = 1, 2, 3$.

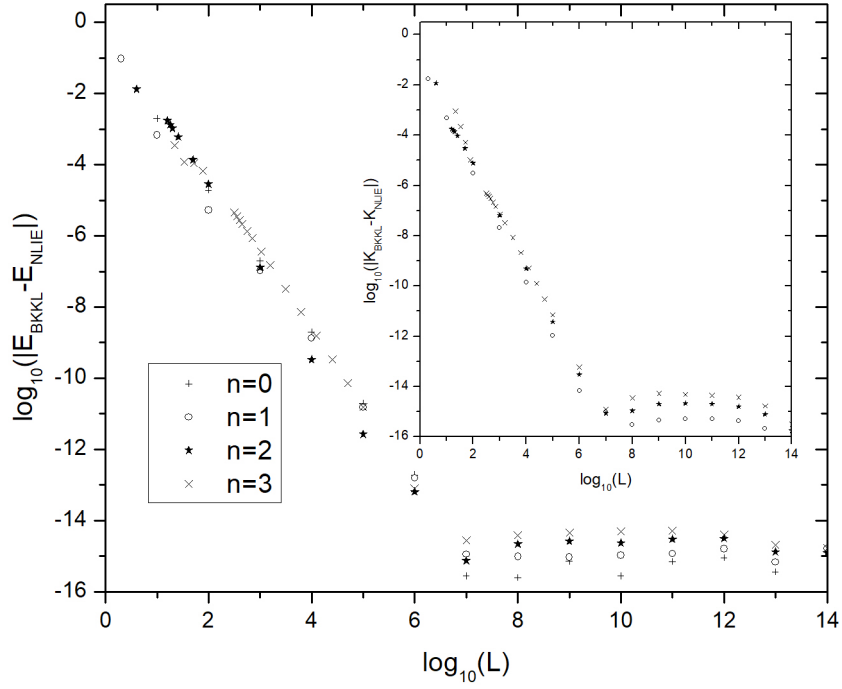


Figure 7: Comparison of the energies E_{NLIE} and quasi-momenta K_{NLIE} (inset) from numerically solving the NLIE (29) with $E_{BKKL} = (2g\gamma/\pi)s^2$ and $K_{BKKL} = 4g\gamma s$ (inset) with s computed from the quantization condition in [15]. Plotted is the difference which vanishes algebraically with system size like $\mathcal{O}(L^{-2})$, but not below values of the order 10^{-15} to 10^{-14} set by the accuracy of our numerical calculations with double precision operations. The parameters were taken to be $\gamma = 0.8$ and $n = 0, 1, 2, 3$.

5 Analytical study of the scaling dimensions

To handle the scaling limit for $L \rightarrow \infty$, we observe that in the NLIEs (18,24) only the driving term explicitly depends on L and possesses the asymptotics

$$L \log \tanh \frac{g}{2} x \simeq -2L e^{-g|x|}, \quad (43)$$

from which we conclude that all functions $a_j(x)$ are extremely small for $|x| < (\log L)/g$ and change to their asymptotic form in the neighbourhood of $x \sim \pm(\log L)/g$. This property may be used to define non-trivial functions in the scaling limit by suitable shifts of the argument by the offset $\pm(\log L)/g$. Here, due to the necessity to work with the functions on the positive and negative real semi-axes at the same time, we avoid these definitions.

We next use the differentiated NLIE with singular kernel

$$(\log a_i)' = d' + \sum_{j=1}^4 K'_{ij} * \log(1 + a_j), \quad (44)$$

which we multiply from left by $\log(A_i(x))$, sum over the index i and integrate along the positive semi-axis

$$\begin{aligned} \int_0^\infty dx \sum_{i=1}^4 \log(A_i(x)) (\log a_i(x))' &= \int_0^\infty dx \sum_{i=1}^4 \log(A_i(x)) d'(x) \\ &+ \frac{1}{2\pi} \int_0^\infty dx \int_{-\infty}^\infty dy \sum_{i,j=1}^4 \log(A_i(x)) K'_{ij}(x-y) \log(A_j(y)). \end{aligned} \quad (45)$$

The next steps consist in showing: (i) the integral on the left hand side can be explicitly evaluated, (ii) the first term on the right hand side is – up to a scale factor – identical to the energy integral in (36), (iii) the second term on the right hand side can also be evaluated. These calculations are done for large system size L and ignore certain higher order terms.

Ad (i): a change of the variable of integration from x to a_i turns the left hand side of (45) into a dilogarithmic integral along the trajectory the function $a_i(x)$ takes from $x = 0$ to $x = +\infty$, namely from $a_i(0) = 0$ to $a_i(+\infty) = 1$. The trajectory itself does not matter as long as it does not wind around the singularities of the integrand, which we assume here. For each i the integral evaluates to $\pi^2/12$, times 4 yielding $\pi^2/3$. The error done is of the order $a_i(0)$, that is exponentially small in L .

Ad(ii): The first term on the right hand side is, with a view to (43) equal to

$$L2g \int_0^\infty dx e^{-gx} [\log A_1(x) + \log A_2(x) + \log A_3(x) + \log A_4(x)], \quad (46)$$

with an error of order $\mathcal{O}(L^{-2})$. The integral in (36) along the positive semi-axis is identical with a different prefactor

$$-\sin(2\gamma) \frac{g^2}{\pi} \int_0^\infty dx e^{-gx} [\log A_1(x) + \log A_2(x) + \log A_3(x) + \log A_4(x)], \quad (47)$$

and an error of order $\mathcal{O}(L^{-3})$.

Ad (iii): Here we use the fact that the kernel matrix $K_{ij}(x-y)$ is symmetric with respect to an exchange of x, i and y, j , and the differentiated kernel $K'_{ij}(x-y)$ is antisymmetric. The second term on the right hand side of (45) can be massaged

$$\int_0^\infty dx \int_{-\infty}^\infty dy \sum_{i,j=1}^4 \dots = \underbrace{\int_0^\infty dx \int_0^\infty dy \sum_{i,j=1}^4 \dots}_{=0} + \int_0^\infty dx \int_{-\infty}^0 dy \sum_{i,j=1}^4 \dots \quad (48)$$

where ... refer to the integrand in (45) with antisymmetry in x, i and y, j and thus the first term with symmetric integrations and sums over x, i and y, j yields zero.

In the second term on the right hand side of (48) the variable of integration is a positive x (negative y). The integrand is only noticeably different from zero for x (y) taking values around $(\log L)/g$ ($(-\log L)/g$) and larger (lower). This means that $K_{ij}(x-y)$ can be replaced by its asymptotic behaviour as it matters only for $x-y$ taking values around $2(\log L)/g$ or larger. Replacing K'_{ij} by the limiting values $(-1)^{i+j}g/2\gamma$ yields

$$\begin{aligned} \int_0^\infty dx \int_{-\infty}^0 dy \sum_{i,j=1}^4 \log(A_i(x)) K'_{ij}(x-y) \log(A_j(y)) &= \frac{g}{2\gamma} \int_0^\infty dx \int_{-\infty}^0 dy \sum_{i,j=1}^4 (-1)^{i+j} \log(A_i(x)) \log(A_j(y)) \\ &= \frac{g}{2\gamma} |I|^2, \end{aligned} \quad (49)$$

where we define (the identity is shown below):

$$I := \int_0^\infty dx \log \left(\frac{A_1(x)A_3(x)}{A_2(x)A_4(x)} \right) = - \int_{-\infty}^0 dx \log \left(\frac{A_1(x)A_3(x)}{A_2(x)A_4(x)} \right). \quad (50)$$

In this way the problem reduces to calculate the integral I , which can be obtained from the NLIE

$$2\pi i n = \log a_1(+\infty) - \log a_1(-\infty) \quad (51)$$

$$= \frac{1}{2\pi} \lim_{x \rightarrow \infty} \int_{-\infty}^\infty dy \sum_{j=1}^4 K_{1j}(x-y) \log(A_j(y)) - \frac{1}{2\pi} \lim_{x \rightarrow -\infty} \int_{-\infty}^\infty dy \sum_{j=1}^4 K_{1j}(x-y) \log(A_j(y)) \quad (52)$$

$$= \frac{g}{4\gamma\pi} \left[\lim_{x \rightarrow \infty} \int_{-\infty}^\infty dy (x-y) \log \left(\frac{A_1(y)A_3(y)}{A_2(y)A_4(y)} \right) + \lim_{x \rightarrow -\infty} \int_{-\infty}^\infty dy (x-y) \log \left(\frac{A_1(y)A_3(y)}{A_2(y)A_4(y)} \right) \right]. \quad (53)$$

From this resp. the existence of the $x \rightarrow \pm\infty$ limits we learn that the integral over $\log[A_1(y)A_3(y)/A_2(y)A_4(y)]$ from $y = -\infty$ to $+\infty$ is zero and drops out. This also proves the identity in (50). The remaining integrals give

$$2\pi i n = \dots = -\frac{g}{2\gamma\pi} \int_{-\infty}^\infty dy y \log \left(\frac{A_1(y)A_3(y)}{A_2(y)A_4(y)} \right) = -\frac{g}{\gamma\pi} \frac{\log L}{g} \cdot I, \quad (54)$$

where we have used in the last step the fact that $\log[A_1(y)A_3(y)/A_2(y)A_4(y)]$ is purely imaginary and non-zero only in the neighborhood of $y = (\log L)/g$. From the last equation we find

$$I = -i \frac{2\pi^2\gamma}{\log L} n, \quad (55)$$

and hence the double integral (48) is

$$\int_0^\infty dx \int_{-\infty}^0 dy \sum_{i,j=1}^4 \log(A_i(x)) K'_{ij}(x-y) \log(A_j(y)) = 2g\gamma \left(\frac{\pi^2 n}{\log L} \right)^2 \quad (56)$$

The leading errors in the calculation of (49) are of order $\mathcal{O}(L^{-(\pi-2\gamma)/\gamma})$ and $\mathcal{O}(L^{-1})$. There is however a special structure of these terms and it seems likely that they recombine and leave (49) correct to high order in powers of L^{-1} with additional terms to I (50). The calculation of I in (55) comes of course with leading errors resulting in changing $\log L$ to a $\log L/L_0$ with some constant L_0 . Summing the above terms (i), (ii), (iii) with the analogues resulting from (45) with integration over x along the negative semi-axis we obtain

$$\frac{2}{3}\pi^2 = -\frac{2\pi L}{g \sin(2\gamma)} (E - Le_0) + \frac{2g\gamma}{\pi} \left(\frac{\pi^2 n}{\log L} \right)^2, \quad (57)$$

which is (40) for $m = w = N = 0$ with (41).

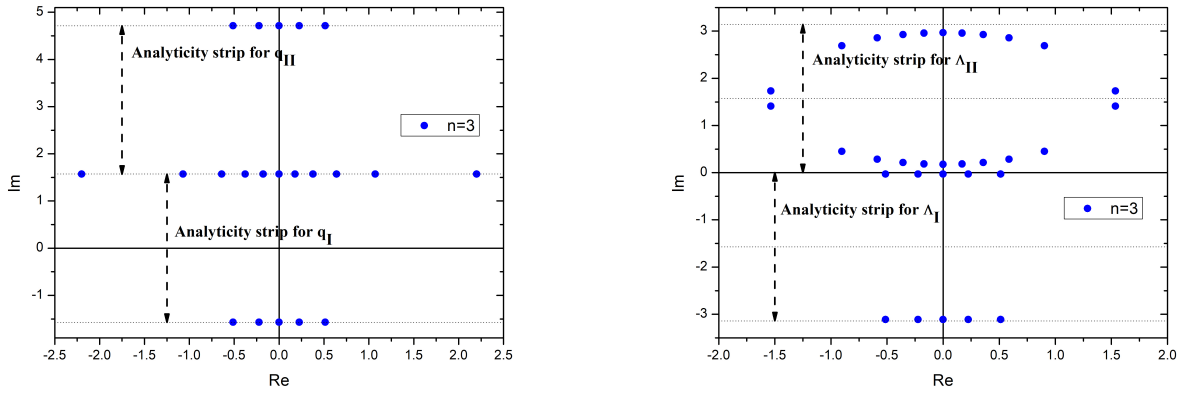


Figure 8: Depiction of the location of all zeros like in Fig. 3 for parameters $L = 16$ and $\gamma = 0.8$. Here the value of $n = 3$ is large against $\log L$ resulting in strong deviations of the zeros of $\Lambda(z)$ from the lines \mathbb{R} and $\mathbb{R} \pm i\pi$. Four of these zeros deviate extremely and have to be treated explicitly as described in the main text. Note that the zeros of $q(z)$ still lie precisely on straight lines.

6 Deformed patterns of root distributions / Descendant states

In this section we study states with root distributions that show qualitative differences in comparison to those shown in Fig. 3. Here we understand by root distribution the distribution of zeros of $q(z)$ and those of $\Lambda(z)$. For such roots not lying in the “standard” regions of the complex plane particular care has to be applied leading to NLIE with additional terms in the driving term, see e.g. [32, 33].

The first such case, interestingly, corresponds to the class of states treated in Sect. 3 resp. Fig. 3, however with a large ratio $n/\log L$. In this case, the zeros of $q(z)$ are still exclusively distributed along the lines $\mathbb{R} \pm i\pi/2$, but some zeros of $\Lambda(z)$ deviate strongly from the lines \mathbb{R} and $\mathbb{R} \pm i\pi$, see Fig. 8, such that the Fourier transforms of the logarithmic derivatives of the Λ functions appearing in (12)-(15) can no longer be reduced to just two independent functions.

Here we treat the case that four zeros, called $\theta_1, \dots, \theta_4$, enter the region of the complex plane with imaginary parts between γ and $\pi - \gamma$. In (12) and (13) the function $\Lambda(z)$ is evaluated on the lines $\mathbb{R} + i\gamma$ and $\mathbb{R} + i(\pi - \gamma)$ with four zeros inbetween. Therefore the Fourier transform of the logarithmic derivatives of these equations does not lead to (A.5) and (A.6) in the appendix. Of course, (A.7) and (A.8) are still valid. Analogous considerations apply for zeros with imaginary parts between $-(\pi - \gamma)$ and $-\gamma$.

There are several ways to proceed in this situation. Here we use subtraction terms. We define

$$\lambda(z) := \prod_{j=1}^4 \sinh \frac{1}{2}(z - \theta_j), \quad (\text{version 1}) \quad (58)$$

as well as modified functions

$$\tilde{A}_1(x) := \frac{A_1(x)}{\lambda(x + i\gamma)}, \quad \tilde{A}_2(x) := \frac{A_2(x)}{\lambda(x + i\pi - i\gamma)}, \quad \tilde{A}_3(x) := \frac{A_3(x)}{\lambda(x - i\gamma)}, \quad \tilde{A}_4(x) := \frac{A_4(x)}{\lambda(x + i\pi + i\gamma)}. \quad (59)$$

These functions satisfy factorizations like (12)-(15) with the only change that $\Lambda(z)$ is replaced by

$$\tilde{\Lambda}(z) := \frac{\Lambda(z)}{\lambda(z)}, \quad (60)$$

which has no zeros in the region discussed above. Hence the Fourier transforms of all equations yield (A.5)-(A.8) where now $\hat{\Lambda}_I, \hat{\Lambda}_{II}$ are the Fourier transforms of the logarithmic derivative of $\tilde{\Lambda}(z)$ in regions I and II. From this again (18) and (19) follow with the only modification that A_j are to be replaced by \tilde{A}_j . The same holds for (24) and (29).

A problem is left with (58), which renders the functions (59) having vanishing asymptotics, so their logarithms have diverging asymptotics. These functions do not allow for the Fourier transform which is necessary for the numerics. Hence we modify the definition (58) – by keeping (59) – to

$$\lambda(z) := \prod_{j=1,3} \frac{\sinh \frac{1}{2}(z - \theta_j)}{\sinh \frac{1}{2}(z - \text{Re } \theta_j)} \prod_{j=2,4} \frac{\sinh \frac{1}{2}(z - \theta_j)}{\sinh \frac{1}{2}(z - \text{Re } \theta_j - \pi i)}, \quad (\text{version 2}), \quad (61)$$

where we assumed that $0 < \text{Im } \theta_{1,3} < \pi/2$ and $\pi/2 < \text{Im } \theta_{2,4} < \pi$.

Now we can use (29) with the replacement of A_j by \tilde{A}_j . Of course the location of all θ_j has to be known. They are determined from the condition $a(\theta_j) = -1$ or for instance from $a_1(\theta_j - i\gamma) = -1$ which is evaluated by use of the NLIEs as integral expressions for the functions $\log a_j(x)$ allowing for complex arguments x .

This program leads to a coupled set of NLIEs and scalar equations for the θ_j . Having solved it, the integral expressions for energy and quasi-momentum have to be evaluated. To this end we may start with (33) and (38) with Λ and A_j replaced by $\tilde{\Lambda}$ and \tilde{A}_j , and then obtain the analogues of (36) and (39) with additional θ_j -terms appearing on the right hand sides. The modified (36) is still an integral over the product of a function with pole of 2nd order in $x = 0$ times the sum over all \tilde{A}_j which, unlike the sum over all A_j does not have a zero of high order at $x = 0$. Therefore, the resulting expressions need to be written in terms of integrals involving the A_j .

The obtained modified versions of (36) and (39) are

$$E = Le_0 + \sum_{j=1}^4 \frac{g \sin(2\gamma)}{\cosh(g(\theta_j - \frac{\pi}{2}i))} - \frac{\sin(2\gamma)}{2\pi} \int_{-\infty}^{\infty} dx \frac{g^2 \cosh gx}{(\sinh gx)^2} \sum_{j=1}^4 \log A_j(x), \quad (62)$$

$$K = \log \left[\prod_{j=1}^4 \sinh(g(\theta_j - i\gamma)) \right] + \frac{g}{2\pi i} \int_{-\infty}^{\infty} dx \coth(gx) \log \left[\tanh^8 \left(\frac{g}{2}x + \frac{\pi}{4}i \right) \cdot \frac{A_1(x)A_3(x)}{A_2(x)A_4(x)} \right], \quad (63)$$

where here indeed the functions A_j enter, not the \tilde{A}_j . We find that equation (62) is obtained most elegantly from the original (36) which also holds in the currently considered case provided the contours for the integrals are suitably deformed. In the convolution integral an integration by parts is carried out resulting in a convolution over the kernel function κ and the derivative of the sum of A_j . Then by use of Cauchy's theorem the deformations are “straightened” upon which contributions of residues appear as the new explicit terms in (62). At last, in the convolution integral with straight contours the integration by parts is run backwards to give (62). For the derivation of (63) we start from (39) with deformed contours and perform an integration by parts where we use $\tilde{\kappa}(x) = i g \coth(gx)$

$$K = \frac{-1}{2\pi i} \int dx (\log \sinh gx) [(\log A_1(x))' - (\log A_2(x))' + (\log A_3(x))' - (\log A_4(x))'], \quad (\text{deformed contours!}). \quad (64)$$

We straighten the deformed contours and obtain

$$K = \sum_{j=1}^4 \log \sinh(g(\theta_j - i\gamma)) - \frac{1}{2\pi i} \int dx (\log \sinh gx) [(\log A_1(x))' - (\log A_2(x))' + (\log A_3(x))' - (\log A_4(x))'], \quad (65)$$

with straight contours. It is tempting to perform directly an integration by parts. However, the resulting integral does not exist, because the function $\log A_1 - \log A_2 + \log A_3 - \log A_4$ has non trivial asymptotics. Adding and subtracting the $\log \tanh$ term appearing in (63) cures the problem: the integral with just the counter term can be done and for argument $x = 0$ yields zero! The remaining integral with the modified second factor allows for integrating by parts.

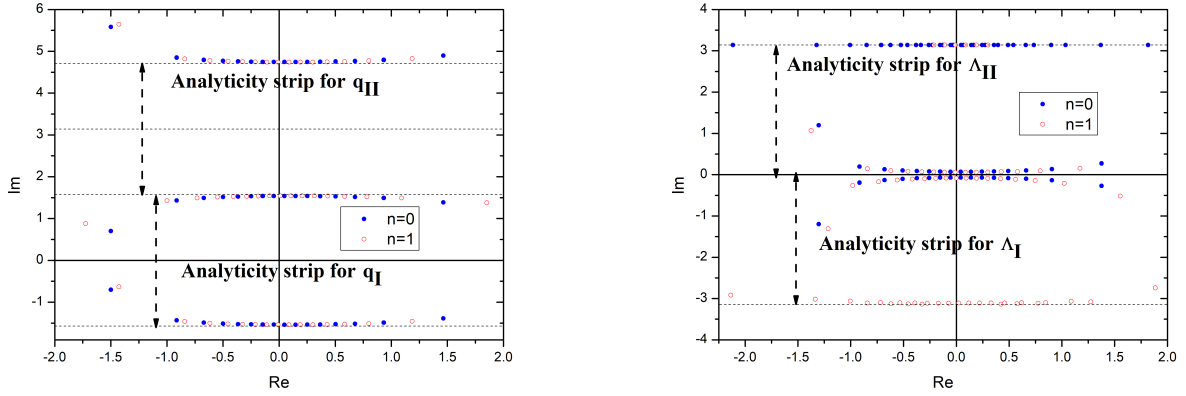


Figure 9: Descendant states with $N = 1$ for $m = w = 0$: Depiction of the location of all zeros in the complex plane for a) the function $q(z)$ and b) the eigenvalue function $\Lambda(z)$. We use parameters $L = 32$ and $\gamma = 0.8$. Disks refer to the lowest lying state in this sector ($n = 0$) and circles to the first excited state ($n = 1$). For these states the zeros of $q(z)$ and the zeros of $\Lambda(z)$ deviate noticeably from the standard distribution lines. The zeros of $q(z)$ with strongest deviation (and largest negative real part) are denoted by z_1, z_2 , the analogous zeros of $\Lambda(z)$ are denoted by θ_1, θ_2 .

This way we obtain (63) with well-defined integral.

Descendant states

Next we treat the first descendant state with $N = 1$ for $m = w = 0$. The distribution of Bethe roots, i.e. the zeros of $q(z)$ are changed qualitatively. The two roots z_1, z_2 with extremal real parts leave the axes with imaginary parts $\pm\pi/2$ and move closer to the real axis as illustrated in Fig. 9. Also the distribution of zeros of $\Lambda(z)$ changes. The two zeros with extremal real parts leave the neighbourhood of the real axis as shown in Fig. 9. As above we define counter terms where we assume $\text{Im } z_1 > 0$, $\text{Im } z_2 < 0$, $\text{Im } \theta_1 > 0$, and $\text{Im } \theta_2 < 0$

$$\begin{aligned} \lambda(z) &:= \frac{\sinh \frac{1}{2}(z - \theta_1) \sinh \frac{1}{2}(z - \theta_2)}{\sinh^2 \frac{1}{2}(z - \frac{1}{2}(\theta_1 + \theta_2))}, \\ q_0(z) &:= \frac{\sinh \frac{1}{2}(z - z_1) \sinh \frac{1}{2}(z - z_2)}{\sinh \frac{1}{2}(z - \text{Re } z_1 - \frac{\pi}{2}i) \sinh \frac{1}{2}(z - \text{Re } z_2 + \frac{\pi}{2}i)}, \\ \alpha(z) &:= \frac{q_0(z - 2i\gamma)}{q_0(z + 2i\gamma)}, \quad \beta(z) := \frac{q_0(z - i\gamma)}{q_0(z + i\gamma)}. \end{aligned} \quad (66)$$

We introduce the modified functions

$$\begin{aligned} \tilde{a}_1(x) &:= \alpha(x + i\gamma)a_1(x), \quad \tilde{a}_2(x) := \frac{a_2(x)}{\alpha(x + i\pi - i\gamma)}, \\ \tilde{a}_3(x) &:= \frac{a_3(x)}{\alpha(x - i\gamma)}, \quad \tilde{a}_4(x) := \alpha(x + i\pi + i\gamma)a_4(x), \end{aligned} \quad (67)$$

and

$$\begin{aligned} \tilde{A}_1(x) &:= \frac{\beta(x)}{\lambda(x + i\gamma)}A_1(x), \quad \tilde{A}_2(x) := \frac{A_2(x)}{\beta(x + i\pi)\lambda(x + i\pi - i\gamma)}, \\ \tilde{A}_3(x) &:= \frac{A_3(x)}{\beta(x)\lambda(x - i\gamma)}, \quad \tilde{A}_4(x) := \frac{\beta(x + i\pi)}{\lambda(x + i\pi + i\gamma)}A_4(x). \end{aligned} \quad (68)$$

These functions satisfy factorizations like (7)-(10) and (12)-(15) with the only change that $q(z)$ and $\Lambda(z)$ are replaced by

$$\tilde{q}(z) := \frac{q(z)}{q_0(z)}, \quad \tilde{\Lambda}(z) := \frac{\Lambda(z)}{\lambda(z)}, \quad (69)$$

which have no zeros in the regions I and II as discussed above. Hence the Fourier transforms of all equations yield (A.5)-(A.8) where now \hat{q}_I, \hat{q}_{II} and $\hat{\Lambda}_I, \hat{\Lambda}_{II}$ are the Fourier transforms of the logarithmic derivatives of $\tilde{q}(z)$ and $\tilde{\Lambda}(z)$ in regions I and II. From this again (18) and (19) follow with the only modification that a_j and A_j are to be replaced by \tilde{a}_j and \tilde{A}_j . The same holds for (24) and (29).

Now we can use (29) with the described replacements. Of course the location of the z_1, z_2 and θ_1, θ_2 has to be known. They are determined from the condition $a(z_j) = -1$ and $a(\theta_j) = -1$ or for instance from $a_1(z_j - i\gamma) = -1$ and $a_1(\theta_j - i\gamma) = -1$ which are evaluated by use of the NLIEs as integral expressions for the functions $\log a_j(x)$ allowing for complex arguments x .

This program leads to a coupled set of NLIEs and scalar equations for the z_j and θ_j . Having solved it, the integral expressions for energy and quasi-momentum have to be evaluated. The modified versions of (36) and (39) are

$$E = Le_0 + \frac{g \sin(2\gamma)}{\cosh(g(\theta_1 - \frac{\pi}{2}i))} + \frac{g \sin(2\gamma)}{\cosh(g(\theta_2 + \frac{\pi}{2}i))} - \frac{\sin(2\gamma)}{2\pi} \int_{-\infty}^{\infty} dx \frac{g^2 \cosh gx}{(\sinh gx)^2} \sum_{j=1}^4 \log A_j(x), \quad (70)$$

$$K = \log \frac{\sinh(g(\theta_1 - i\gamma))}{\sinh(g(\theta_2 + i\gamma))} + \frac{g}{2\pi i} \int_{-\infty}^{\infty} dx \coth(gx) \log \left(\frac{A_1(x)A_3(x)}{A_2(x)A_4(x)} \right). \quad (71)$$

In Fig. 10 and Fig. 11 we show the real and imaginary parts of the above introduced functions for the descendant states with $n = 0$ and $n = 1$.

Fig. 12 shows data obtained by our NLIE approach for the descendant states compared to the ODE/IQFT results [15]. We see the difference of the two approaches is best fitted by an order $\mathcal{O}(L^{-2})$ ansatz. Here, for the descendant states with $N = 1$ and $m = w = 0$ the quality of our numerical data is slightly worse than in the case of the primary states with $N = 0$ and $m = w = 0$. This is understood from the numerics and the “richer features” of the solution functions for the case $N = 1$ rendering the numerical Fourier transforms less accurate. The form of the graphs of the functions is the limiting factor, not the additional task to determine the positions of the θ_j parameters. Their numbers appear to be rather stable in various different runs of the iterative solution routine with different parameters for the width of the interval and number of grid points chosen. Note however, that for large system sizes the agreement between the NLIE and the ODE/IQFT results for the quasi-momentum approaches 14 decimal digits. In case of the energy the agreement between the results becomes worse for system sizes larger than 10^6 , see Fig. 12. This we attribute to the more susceptible dependence of (70) to numerical inaccuracies in comparison to (71).

7 Conclusion

In this paper, we have investigated the spectral properties of the staggered six-vertex model with \mathbb{Z}_2 symmetry ($\alpha = \pi/2$) for arbitrary system sizes L using non-linear integral equations (NLIEs). Our study builds on the important works of Candu and Ikhlef [21] and Frahm and Seel [22], who were the first to address this topic and yielded significant results in both the scaling limit and for finite, relatively large system sizes.

Our research was motivated by two primary questions. The first question concerned the accuracy of results based on the ODE/IQFT correspondence, which holds in the asymptotic regime of large system sizes L . We found that the quantization conditions for the low-lying primary states as obtained in [8] and improved and extended to descendant states in the comprehensive work of Bazhanov, Kotousov, Koval, and Lukyanov [15, 16, 23], are impressively accurate even for relatively small sizes. In the anisotropy parameter range $\pi/4 < \gamma < \pi/2$, the difference between NLIE and ODE/IQFT results for the energy and quasi-momentum eigenvalues vanishes in the scaling limit as $\mathcal{O}(L^{-2})$.

The second question we explored was whether there exists an optimal NLIE-based approach for studying the staggered six-vertex model. The linear and non-linear integral equations in [8] and [21], respectively, feature singular

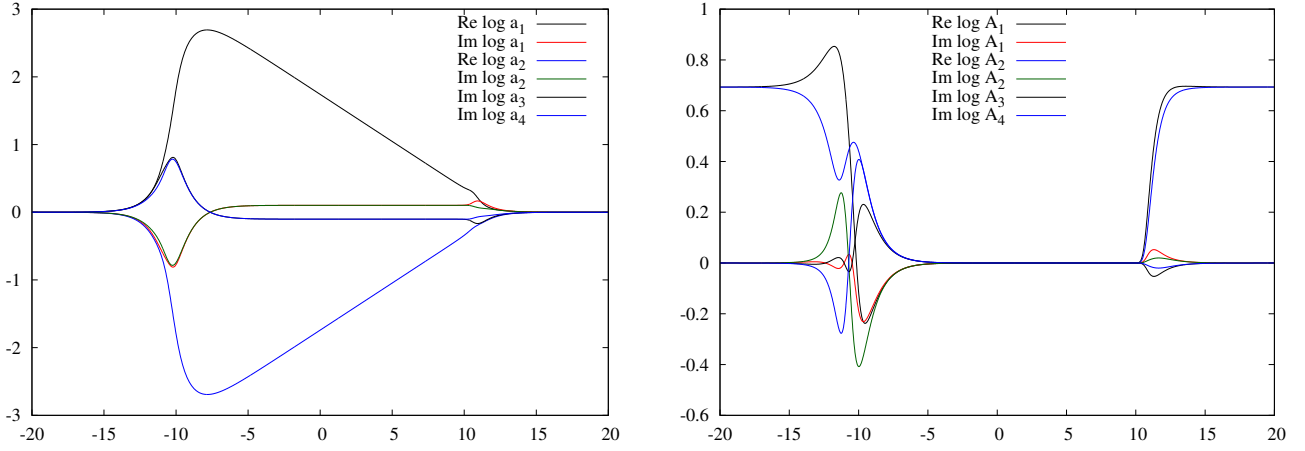


Figure 10: The first descendant state with $L/2 - 1$ roots located close to the upper as well as to the lower axis $\mathbb{R} \pm i\pi/2$ ($n = 0$): a) Depiction of real and imaginary parts of the functions $\log \tilde{a}_j - d$ with $j = 1, 2, 3, 4$, see (67). The real parts for $i = 1, 3$ ($i = 2, 4$) are identical and shown by a black (blue) line. Similar depiction of the functions $\log \tilde{A}_i$, see (68). We use parameters $L = 10^{10}$ and $\gamma = 0.9$.

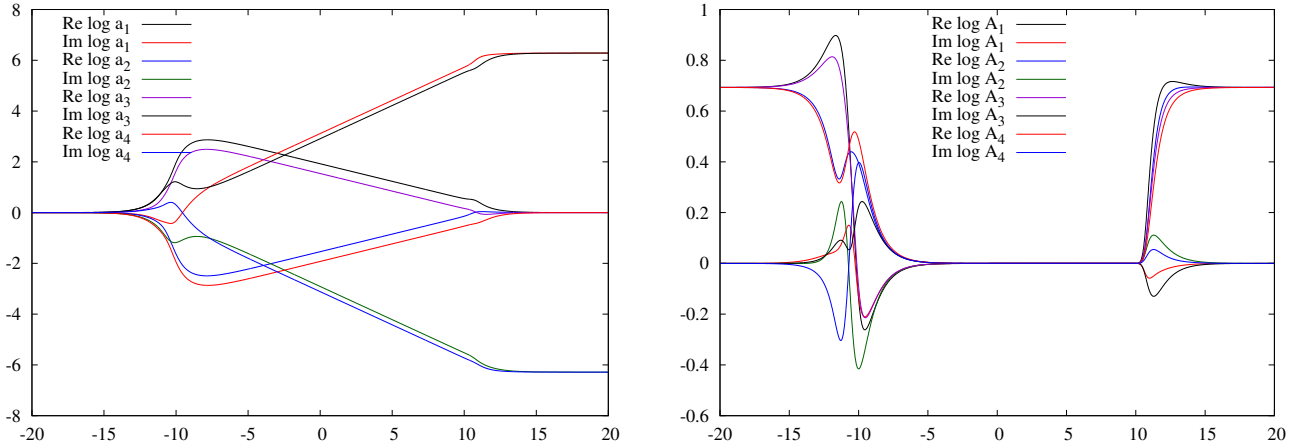


Figure 11: The second descendant state with $L/2$ roots located close to the upper and $L/2 - 2$ roots close to the lower axis ($n = 1$): a) Depiction of real and imaginary parts of the functions $\log \tilde{a}_j - d$ with $j = 1, 2, 3, 4$, see (67). Similar depiction of the functions $\log \tilde{A}_i$, see (68). We use parameters $L = 10^{10}$ and $\gamma = 0.9$.

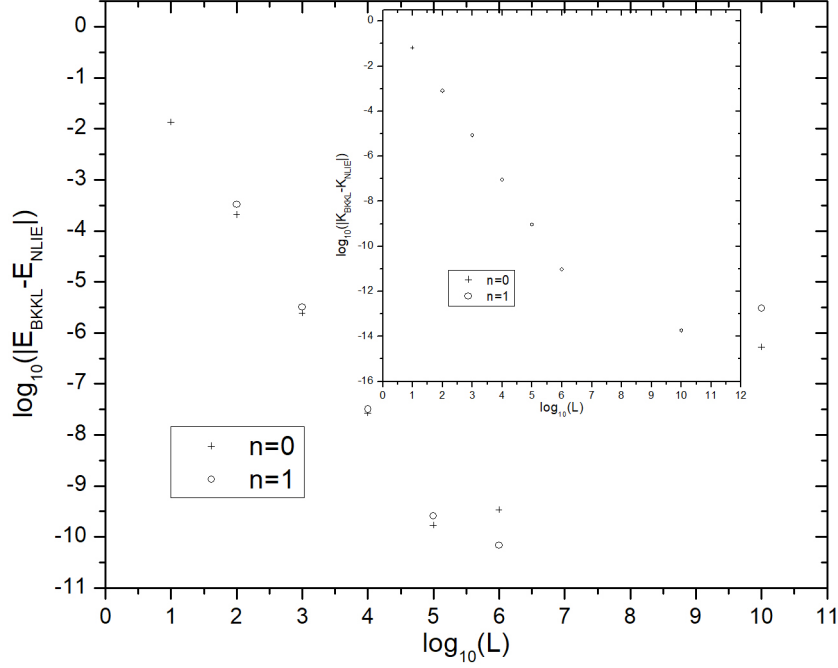


Figure 12: Comparison of the energies E_{NLIE} and quasi-momenta K_{NLIE} for the descendant states with $E_{BKKL} = (2g\gamma/\pi)s^2$ and $K_{BKKL} = 4g\gamma s$ with s computed from the quantization condition in [15]. The parameters were taken to be $\gamma = 0.9$ and $n = 0, 1$. Plotted is the difference which vanishes algebraically with system size like $\mathcal{O}(L^{-2})$, but not below values of the order 10^{-10} (10^{-14}) for the energy (quasi-momentum) data. Our numerical calculations for the NLIEs were done with double precision operations. The accuracy of the quasi-momentum data is higher than that for the energy data: The values of the quasi-momentum depend largely on the “shape” of the functions $\log A_j(x)$ as shown in Fig. 10 and Fig. 11. Note the transition of the functions between the asymptotic values 0 and $\log(2)$ in regions $x \simeq \pm(\log L)/g$. The values of the energy depend sensitively on the precise location of this transition.

kernels, whereas those in [22] have regular kernels. We analyzed why this occurs and how different versions of NLIE are related. We presented a compact derivation of NLIE with a singular kernel, which is directly equivalent to that in [8]. By rearranging terms, we obtained an equivalent set of NLIE with a regular kernel. This version of NLIE still “retains some memory” of the issues presented by the singular kernel version. While the convolution integrals in the numerical treatment are well-defined, the iterative procedure of the basic version of the regular kernel NLIE converges only for carefully designed initial data.

Both versions of NLIE, singular and regular, are valid for all states with an arbitrary number n of Bethe roots reallocated between the distribution lines $\mathbb{R} \pm i\pi/2$, where n does not appear in the driving terms of the NLIE. Naturally, the singular kernel NLIE introduces additional challenges. In the regular kernel version, the kernel is not applied to the four functions $\log A_j$, which take small values, but to the combination $\log a_j - d - 2\log A_j$, which has non-vanishing asymptotes due to the winding of the trajectories of the functions $a_j(x)$ in the complex plane. The value of the windings is $\pm n$, meaning the imaginary parts of $\log a_j(x)$ increase by $\pm n \cdot 2\pi$ between $x = -\infty$ and $x = +\infty$. By incorporating this information, the regular kernel NLIE can be supplemented with counterterms to allow for stable numerical solutions via iterative methods. Since all functions entering the convolution integrals take small values, the numerical results are highly accurate, up to nearly all available digits (with a minor loss due to the large number of grid points).

We successfully performed calculations for lattice sizes ranging from $L = 2$ to $L = 10^{24}$. For $L = 2$ to $L = 10^6$, the agreement with the ODE/IQFT results increased, with deviations of the order of $\mathcal{O}(L^{-2})$. Beyond $L = 10^6$, the differences remained around 10^{-15} to 10^{-14} due to the “limited” numerical precision available. We assert that the results of the NLIE-based calculations are numerically exact.

We also elucidated the relationship between our regular version of NLIE and that of [22]. A modified and slightly asymmetric variant of our transformation from the singular kernel version to regular kernel versions yields the results of [22]. Finally, we demonstrated how to derive analytic results for the scaling limit within the NLIE approach. Interestingly, the singular version of NLIE is extremely useful in this context, allowing for the application of the dilogarithmic trick [25], which yields the leading logarithmic term in the conformal weights. These calculations are conducted without any Wiener-Hopf techniques, using instead only elementary manipulations and the winding of the involved functions.

Many open questions remain, particularly regarding the derivation of all higher-order terms identified by [15]. Possibly similar NLIE may allow for calculating the spectrum of the complex sinh-Gordon model where in the lattice regularization the inhomogeneities contain a staggering not only along the imaginary but also in the real direction.

Acknowledgments

We acknowledge financial support by Deutsche Forschungsgemeinschaft through FOR 2316. We thank Y. Ikhlef, J. Jacobsen, H. Frahm, S. Gehrman, G. Kotousov, S. Lukyanov, and H. Saleur for stimulating discussions and insightful perspectives on the topic. AK gratefully acknowledges support from the Simons Center for Geometry and Physics, Stony Brook University at which some of the research for this paper was performed. AK also gratefully acknowledges support through the PIFI fellowship by the Chinese Academy of Sciences and the Innovation Academy for Precision Measurement Science and Technology, Wuhan, where the final calculations and writing were completed.

A Fourier transform

By use of a short hand notation for the Fourier transform of the logarithmic derivative of a function $f(x)$ as $\hat{f} := \mathfrak{F}_k\{\frac{d}{dx} \log f(x)\}$ we list the Fourier transforms of the logarithmic derivatives of the eight multiplicative relations (7)-(10) and (12)-(15)

$$\hat{a}_1 = \left(1 - e^{-2\gamma k}\right) \hat{\Phi} + e^{-3\gamma k} \hat{q}_{II} - e^{\gamma k} \hat{q}_I, \quad (\text{A.1})$$

$$\hat{a}_2 = \left(1 - e^{(2\gamma-\pi)k}\right) \hat{\Phi} + e^{(3\gamma-\pi)k} \hat{q}_I - e^{-(\gamma+\pi)k} \hat{q}_{II}, \quad (\text{A.2})$$

$$\hat{a}_3 = \left(1 - e^{(2\gamma-\pi)k}\right) \hat{\Phi} + e^{(3\gamma-2\pi)k} \hat{q}_{II} - e^{-\gamma k} \hat{q}_I, \quad (\text{A.3})$$

$$\hat{a}_4 = \left(1 - e^{-2\gamma k}\right) \hat{\Phi} + e^{(\pi-3\gamma)k} \hat{q}_I - e^{(\gamma-\pi)k} \hat{q}_{II}, \quad (\text{A.4})$$

and

$$\hat{A}_1 = -e^{-2\gamma k} \hat{\Phi} + e^{-\gamma k} \hat{q}_I - e^{\gamma k} \hat{q}_I + e^{-\gamma k} \hat{\Lambda}_{II}, \quad (\text{A.5})$$

$$\hat{A}_2 = -e^{(2\gamma-\pi)k} \hat{\Phi} + e^{(\gamma-\pi)k} \hat{q}_{II} - e^{-(\gamma+\pi)k} \hat{q}_{II} + e^{(\gamma-\pi)k} \hat{\Lambda}_{II}, \quad (\text{A.6})$$

$$\hat{A}_3 = -e^{(2\gamma-\pi)k} \hat{\Phi} + e^{\gamma k} \hat{q}_I - e^{-\gamma k} \hat{q}_I + e^{\gamma k} \hat{\Lambda}_I, \quad (\text{A.7})$$

$$\hat{A}_4 = -e^{-2\gamma k} \hat{\Phi} + e^{-(\gamma+\pi)k} \hat{q}_{II} - e^{(\gamma-\pi)k} \hat{q}_{II} + e^{(\pi-\gamma)k} \hat{\Lambda}_I, \quad (\text{A.8})$$

where we have explicitly

$$\hat{\Phi} = -iL \frac{e^{\pi k}}{e^{\pi k} - 1}. \quad (\text{A.9})$$

These equations can be solved for $\hat{a}_1, \dots, \hat{a}_4, \hat{q}_I, \hat{q}_{II}, \hat{\Lambda}_I, \hat{\Lambda}_{II}$ in terms of $\hat{A}_1, \dots, \hat{A}_4, \hat{\Phi}$. The results for $\hat{a}_1, \dots, \hat{a}_4$ are given in (18)-(23). Here we give the result for the Fourier transform of the first logarithmic derivative of the function on the left hand side of (33) and (38)

$$e^{(\gamma-\pi)k} \hat{\Lambda}_{II} + e^{\gamma k} \hat{\Lambda}_I = -iL \frac{\cosh((2\gamma-\pi/2)k)}{\cosh((\pi/2-\gamma)k) \sinh((\pi/2)k)} e^{(\gamma-\pi/2)k} + \frac{e^{(\gamma-\pi/2)k}}{2 \cosh((\pi/2-\gamma)k)} (\hat{A}_1 + \hat{A}_2 + \hat{A}_3 + \hat{A}_4), \quad (\text{A.10})$$

$$e^{(\gamma-\pi)k} \hat{\Lambda}_{II} - e^{\gamma k} \hat{\Lambda}_I = \frac{e^{(\gamma-\pi/2)k}}{2 \sinh((\pi/2-\gamma)k)} (\hat{A}_1 - \hat{A}_2 + \hat{A}_3 - \hat{A}_4). \quad (\text{A.11})$$

The integrated inverse Fourier transform of this yields (33) and (38).

The Fourier transform of the singular kernel needs additional “definitions” for the treatment of the singularity. As it stands the kernel K in (21) with (22) and (23) does not allow for the (inverse) Fourier transform. Of course the second derivative of this function, resp. $K(k)$ multiplied by $-k^2$, can be Fourier transformed. Hence all reasonable definitions of the Fourier transform will differ just by linear terms in x and constants. This freedom of definition does not imply that the solution to the integral equation (18) is lacking uniqueness. Of course, the treatment requires care resp. a reformulation as presented in Sect. 4.

We want to give the (inverse) Fourier transform of $1/[2 \sinh(\gamma k) \sinh((\pi-2\gamma)k)]$, however for generic γ this is difficult and as intermediate goal we treat $1/[2 \sinh^2(\gamma k)]$ by taking the k -integration contour \mathcal{C} just below the real axis. For the evaluation of the transform we deform the contour into the upper half-plane to $\mathcal{C} + i\pi/\gamma$. Inbetween there is the pole of second order at $k = 0$ which leads to an explicit contribution

$$I(k) := \int_{\mathcal{C}} dk \frac{e^{ikx}}{2 \sinh^2(\gamma k)} = -\frac{\pi x}{\gamma^2} + e^{-\frac{\pi}{\gamma}x} \cdot I(k), \quad (\text{A.12})$$

and a remaining integral of the same form as on the left hand side, because the shift of the contour goes into the exponential in the integrand and yields a k -independent factor. From the last equation we get

$$\int_{\mathbb{C}} dk \frac{e^{ikx}}{2 \sinh^2(\gamma k)} = -\frac{\pi x}{\gamma^2 \left(1 - e^{-\frac{\pi}{\gamma}x}\right)}, \quad (\text{A.13})$$

with asymptotic behaviour $-(\pi/\gamma^2)x$ for large positive values of x , and 0 for large negative x .

With regard to the function of our interest we see from

$$\frac{1}{2 \sinh(\gamma k) \sinh((\pi - 2\gamma)k)} = \frac{g\gamma}{\pi} \frac{1}{2 \sinh^2(\gamma k)} + \mathcal{O}(1/k), \quad g = \frac{\pi}{\pi - 2\gamma}, \quad (\text{A.14})$$

that the asymptotics of the (inverse) Fourier transform is

$$-(g/\gamma)x \quad \text{for large positive } x, \quad 0 \quad \text{for large negative } x, \quad (\text{A.15})$$

and possibly additive constants. The next leading terms are of order $\exp(-(\pi/\gamma)|x|)$ and $\exp(-g|x|)$.

B ODE/IQFT results

The ODE/IQFT analysis [15] yields the following quantization condition for s . For arbitrary integer n

$$8s \log \left(\frac{2L\Gamma(\frac{3}{2} + \frac{1}{\zeta})}{\sqrt{\pi}\Gamma(1 + \frac{1}{\zeta})} \right) + \delta(s) - 2\pi n = 0, \quad (\zeta := \pi/\gamma - 2), \quad (\text{B.1})$$

where the 0 on the right hand side is actually an undetermined $\mathcal{O}((\log L)^{-\infty})$ term. For the primary state $N = 0$ with $m = w = 0$, the phase shift δ entering the above equation is explicitly given by the formula [8, 15]

$$\delta(s) = \frac{16s}{n} \log(2) - 4 \log \left(2^{2s} \frac{\Gamma(\frac{1}{2} - s)}{\Gamma(\frac{1}{2} + s)} \right). \quad (\text{B.2})$$

For the non-primary state with $N = 1$, the explicit formulae for δ are

$$\delta_{\pm} = -4 \log \left(2^{\frac{2s}{\zeta}(\zeta+2)} \frac{\Gamma(\frac{1}{2} - s)}{\Gamma(\frac{1}{2} + s)} \frac{1 - 2s}{1 + 2s} \right) - 2 \log \left(\frac{2\zeta\omega_{\pm} - (\zeta+2)(\zeta-2s)}{2n\omega_{\pm} + (\zeta+2)(\zeta+2s)} \right),$$

where

$$\omega_{\pm} = -\frac{\zeta+1}{2\zeta} \left(2s \pm \sqrt{\zeta(\zeta+2) - 4s^2} \right). \quad (\text{B.3})$$

References

- [1] M. Jimbo, T. Miwa, and F. Smirnov. *Local Operators in Integrable Models I*. Vol. 256. AMS, 2021.
- [2] H. Boos, M. Jimbo, T. Miwa, and F. Smirnov. “Hidden Grassmann Structure in the XXZ Model IV: CFT limit”. In: *Commun. Math. Phys.* 299 (2010), p. 825. arXiv: hep-th/0911.3731.
- [3] R. Vasseur and J. Moore. “Nonequilibrium quantum dynamics and transport: from integrability to many-body localization”. In: *J. Stat. Mech.* (2016), p. 064010. arXiv: cond-mat/1603.06618.

- [4] A. Bayat, S. Bose, and H. Johannesson, eds. *Entanglement in spin chains: from theory to quantum technology applications*. Springer, 2022.
- [5] R. J. Baxter. “Generalized ferroelectric model on a square lattice”. In: *Stud. Appl. Math.* 50 (1971), p. 51.
- [6] J. L. Jacobsen and H. Saleur. “The antiferromagnetic transition for the square-lattice Potts model”. In: *Nucl. Phys. B* 743 (2006), pp. 207–248. arXiv: cond-mat/0512058.
- [7] Y Ikhlef, J L Jacobsen, and H Saleur. “A staggered six-vertex model with non-compact continuum limit”. In: *Nucl. Phys. B* 789 (2008), pp. 483–524.
- [8] Y. Ikhlef, J. L. Jacobsen, and H. Saleur. “An integrable spin chain for the $SL(2, \mathbb{R})/U(1)$ black hole sigma model”. In: *Phys. Rev. Lett.* 108 (2012), p. 081601. arXiv: hep-th/1109.1119.
- [9] S. Elitzur, A. Forge, and E. Rabinovici. “Some global aspects of string compactifications”. In: *Nuclear Physics B* 359.2-3 (1991), pp. 581–610. DOI: 10.1016/0550-3213(91)90073-7.
- [10] G. Mandal, A. M. Sengupta, and S. R. Wadia. “Classical solutions of 2-dimensional string theory”. In: *Mod. Phys. Lett. A* 6 (1991), pp. 1685–1692.
- [11] Edward Witten. “String theory and black holes”. In: *Physical Review D* 44.2 (1991), p. 314. DOI: 10.1103/PhysRevD.44.314.
- [12] R. Dijkgraaf, H. L. Verlinde, and E. P. Verlinde. “String propagation in black hole geometry”. In: *Nucl. Phys. B* 371 (1992), pp. 269–314.
- [13] Juan Maldacena, Hiroshi Ooguri, and John Son. “Strings in AdS_3 and the $SL(2, \mathbb{R})$ WZW model. II: Euclidean black hole”. In: *Journal of Mathematical Physics* 42.7 (2001), pp. 2961–2977. DOI: 10.1063/1.1377039. URL: <https://doi.org/10.1063/1.1377039>.
- [14] A. Hanany, N. Prezas, and J. Troost. “The partition function of the two-dimensional black hole conformal field theory”. In: *Journal of High Energy Physics* 2002.04 (2002), p. 014. URL: <https://iopscience.iop.org/article/10.1088/1126-6708/2002/04/014>.
- [15] Vladimir V. Bazhanov, Gleb A. Kotousov, Sergii M. Koval, and Sergei L. Lukyanov. “On the scaling behaviour of the alternating spin chain”. In: *Journal of High Energy Physics* 2019.087 (2019). DOI: 10.1007/JHEP08(2019)087. URL: [https://doi.org/10.1007/JHEP08\(2019\)087](https://doi.org/10.1007/JHEP08(2019)087).
- [16] Vladimir V. Bazhanov, Gleb A. Kotousov, Sergii M. Koval, and Sergei L. Lukyanov. “Scaling limit of the Z_2 invariant inhomogeneous six-vertex model”. In: *Nuclear Physics B* 965 (2021), p. 115337. DOI: 10.1016/j.nuclphysb.2021.115337.
- [17] Vladimir V. Bazhanov, Gleb A. Kotousov, and Sergei L. Lukyanov. “Equilibrium density matrices for the 2D black hole sigma models from an integrable spin chain”. In: *Journal of High Energy Physics* 2021 (2021), p. 169. DOI: 10.1007/JHEP03(2021)169. URL: [https://doi.org/10.1007/JHEP03\(2021\)169](https://doi.org/10.1007/JHEP03(2021)169).
- [18] Y Ikhlef, J L Jacobsen, and H Saleur. “The Z_2 staggered vertex model and its applications”. In: *Journal of Physics A: Mathematical and Theoretical* 43.22 (2010), p. 225201. DOI: 10.1088/1751-8113/43/22/225201. URL: <https://doi.org/10.1088/1751-8113/43/22/225201>.
- [19] Holger Frahm and Márcio J. Martins. “Finite size properties of staggered $U_q[sl(2|1)]$ superspin chains”. In: *Nuclear Physics B* 847.1 (2011), pp. 220–246. DOI: 10.1016/j.nuclphysb.2011.01.026. URL: <https://doi.org/10.1016/j.nuclphysb.2011.01.026>.
- [20] Holger Frahm and Márcio J. Martins. “Phase diagram of an integrable alternating $U_q[sl(2|1)]$ superspin chain”. In: *Nuclear Physics B* 862.2 (2012), pp. 504–552. DOI: 10.1016/j.nuclphysb.2012.04.019. URL: <https://doi.org/10.1016/j.nuclphysb.2012.04.019>.

- [21] Constantin Candu and Yacine Ikhlef. “Nonlinear integral equations for the $SL(2, \mathbb{R})/U(1)$ black hole sigma model”. In: *Journal of Physics A: Mathematical and Theoretical* 46.41 (Sept. 2013), p. 415401. DOI: 10.1088/1751-8113/46/41/415401. arXiv: hep-th/1306.2646. URL: <https://dx.doi.org/10.1088/1751-8113/46/41/415401>.
- [22] Holger Frahm and Alexander Seel. “The staggered six-vertex model: Conformal invariance and corrections to scaling”. In: *Nuclear Physics B* 879 (2014), pp. 382–406. ISSN: 0550-3213. DOI: <https://doi.org/10.1016/j.nuclphysb.2013.12.015>. URL: <https://www.sciencedirect.com/science/article/pii/S0550321313006044>.
- [23] Vladimir V. Bazhanov, Gleb A. Kotousov, Sergii M. Koval, and Sergei L. Lukyanov. “Some Algebraic Aspects of the Inhomogeneous Six-Vertex Model”. In: *SIGMA* 17 (2021), p. 025. DOI: 10.3842/SIGMA.2021.025. arXiv: 2010.10615 [math-ph]. URL: <https://doi.org/10.3842/SIGMA.2021.025>.
- [24] Gleb A. Kotousov and Sergei L. Lukyanov. “On the scaling behaviour of an integrable spin chain with Z_r symmetry”. In: *Nuclear Physics B* 993 (2023), p. 116269. DOI: 10.1016/j.nuclphysb.2023.116269. URL: <https://doi.org/10.1016/j.nuclphysb.2023.116269>.
- [25] A Klümper, M T Batchelor, and P A Pearce. “Central charges of the 6- and 19-vertex models with twisted boundary conditions”. In: *Journal of Physics A: Mathematical and General* 24.13 (July 1991), p. 3111. DOI: 10.1088/0305-4470/24/13/025. URL: <https://dx.doi.org/10.1088/0305-4470/24/13/025>.
- [26] A. Klümper and M. T. Batchelor. “An Analytic treatment of finite-size corrections in the spin-1 antiferromagnetic XXZ chain”. In: *Journal of Physics A: Mathematical and General* 23 (1990), pp. L189–L195.
- [27] A. Klümper. “Free energy and correlation lengths of quantum chains related to restricted solid-on-solid lattice models”. In: *Annalen der Physik* 1 (1992), pp. 540–553.
- [28] C. Destri and H. J. de Vega. “New thermodynamic Bethe ansatz equations without strings”. In: *Phys. Rev. Lett.* 69 (16 1992), pp. 2313–2317. DOI: 10.1103/PhysRevLett.69.2313.
- [29] C. Destri and H. J. de Vega. “Unified Approach to Thermodynamic Bethe Ansatz and Finite Size Corrections for Lattice Models and Field Theories”. In: *Nucl. Phys. B* 438 [FS] (Apr. 1995), p. 413.
- [30] J. Suzuki. “Spinons in magnetic chains of arbitrary spins at finite temperatures”. In: *Journal of Physics A: Mathematical and General* 32.12 (1999), p. 2341. DOI: 10.1088/0305-4470/32/12/008. URL: <https://iopscience.iop.org/article/10.1088/0305-4470/32/12/008>.
- [31] Jens Damerau and Andreas Klümper. “Nonlinear integral equations for the thermodynamics of the $sl(4)$ -symmetric Uimin-Sutherland model”. In: *Journal of Statistical Mechanics: Theory and Experiment* 2006.12 (Dec. 2006), P12014. DOI: 10.1088/1742-5468/2006/12/P12014. URL: <https://dx.doi.org/10.1088/1742-5468/2006/12/P12014>.
- [32] Andreas Klümper. “Thermodynamics of the Anisotropic Spin-1/2 Heisenberg Chain and Related Quantum Chains”. In: *Z. Physik B* 91.4 (1993), p. 507.
- [33] Changrim Ahn, Zoltan Bajnok, Rafael I. Nepomechie, Laszlo Palla, and Gabor Takacs. “NLIE for hole excited states in the sine-Gordon model with two boundaries”. In: *Nuclear Physics B* 714 (2005), pp. 307–335. DOI: 10.1016/j.nuclphysb.2005.02.004. arXiv: hep-th/0501047 [hep-th].